Supplementary material

Removal of the ionophore antibiotic narasin using vegetal materials as bioadsorbents

Samiha Hamdi[a,b,c], Manel Issaoui[c,d], Ainoa Míguez-González[b], Raquel Cela-Dablanca[b], Sonia Hammami[c], Ana Barreiro[b,*], María J. Fernández-Sanjurjo[b], Esperanza Álvarez-Rodríguez[b], Avelino Núñez-Delgado[b]

[a]Department of Biotechnology, Faculty of Science and Technology of Sidi Bouzid, University of Kairouan, 9100 Sidi Bouzid, Tunisia

[b]Department Soil Science and Agricultural Chemistry, Engineering Polytechnic School, University of Santiago de Compostela, 27002 Lugo, Spain

[c]Laboratory of Nutrition – Functional Foods and Health (NAFS)-LR12ES05, Faculty of Medicine, University of Monastir, Avenue Avicenne 5019 Monastir, Tunisia

[d]Higher Institute of Applied Studies in Humanities of Sbeitla, University of Kairouan, Kasserine, Tunisia

* Correspondence author: Ana Barreiro (ana.barreiro.bujan@usc.es)

1. Additional details on sampling of agro-forest bioadsorbents

In this study, a total of fourteen by-products from various regions of Tunisia were collected in March 2023 (Table S1), whereby the sampling period varied depending on the seasonality of each by-product.

Table S1. Studied biomaterials with their abbreviations and corresponding sampling areas.

Samples	Sampling areas	Abbreviations
Alfa (*Stipa tenacissima)* fiber	The Hadej region (Menzel Bouzaiane, Sidi Bouzid, Central Tunisia)	AF
Cactus (*Opuntia ficus-indica*) fiber	Sampled from the Tala region (Kasserine, North-central Tunisia	CF
Palm (*Phœnix dactylifera* L.) fiber	The Midass region (Tozeur, Southern Tunisia)	PF
Posidonia oceanica fiber	Collected from Skanes beach in the Monastir governorate (eastern coast of Tunisia).	POF
Acacia (*Acacia salicina)* bark	The Maknessy region (Sidi Bouzid governorate, Central Tunisia)	AB
Eucalyptus (*Eucalyptus camaldulensis)* bark		EB
Zean (*Quercus canariensis* Willd) oak bark	The Tabarka region (Northwestern Tunisia)	ZOB
Orange (*Citrus sinensis)* peel	Obtained from a fresh juice shop in the Sidi Bouzid governate (central Tunisia)	OP
Pomegranate (*Punica granatum)* peel	Coming from various pomegranate fields located in the agricultural regions of Gabés governorate (southern Tunisia)	PGP
Pea (*Pisum Sativum)* shell	Sampled from agricultural areas situated in Beja governate (Northwestern Tunisia)	PS
Almond (*Prunus dulcis)* shell	Obtained from almond trees cultivated in the region of Maknessy (Sidi Bouzid, Tunisia)	AS
Date palm (*Phœnix dactylifera* L) stones	Coming from the oasis of Eden palm group (Tozeur, southern Tunisia)	DPS
Coffee grounds (a mixture of 6 samples from different commercial coffee brands available in Tunisia, including Ben Yedder, Bondin, Ellouze, Melita, Gimoka, and Grand Mère)	Yielded from various local coffee outlets in the Maknessy region (central Tunisia)	CGs
Calcined coffee grounds	Prepared by calcining the coffee grounds at 400 ° C for 2 hours.	CC

2. Molecular structure and physicochemical characteristics of NAR antibiotic

Fig. S1 presents the molecular structure of narasin, the ionophore antibiotic investigated in this work.

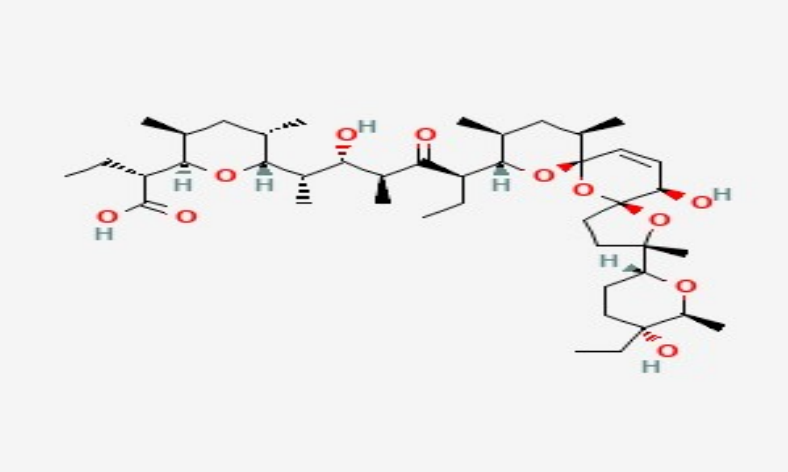

Figure S1. Molecular structure of the ionophore antibiotic narasin (PubChem, CID 65452).

In addition, Table S2 summarizes the physicochemical properties of the studied antibiotic, narasin (NAR, CAS No 55134-13-9, produced by *Streptomyces Auriofaciens*.[1] This acidic polyether ionophore has a molecular formula of C_{43} H_{72} O_{11} and a molar mass of 765.038 g mol^{-1},[1] with the logarithm of its octanol-water partition coefficient (log K_{ow}) ranges from 4.85 to > 6.2 (Table S2).[2] It has a dissociation constant (pK_a, in water) of 4.4 and a low to moderate water solubility (between 102 to 681 mg L^{-1}),[2] similar to those documented for lasalocid (LAS), another acidic anticoccidial,[3] and therefore presents as a cation (pH < pK_a) or anion (pH > pK_a), depending on the pH solution.

Table S2. Main physicochemical proprities of the antibiotic Narasin. $pK_{a:}$ acid dissociation constant calculated by Bak et al. (2013)[4] using Marvinsketch™; K_{oc}: organic carbon partition coefficient; K_{ow}: octanol-water coefficient of partition.

Molar weight (g mol^{-1})	CAS No	Molecular Formula	Solubility in water (mg L^{-1})	pk_a	Stability	Produced by	Log K_{oc}	Log K_{ow}	Soil DT^{50}
765[a]	55134-13-9[a]	$C_{43}H_{72}O_{11}$[a]	102 to 681[b]	4.4[c]	Unstable in Acidic condition, stable in alkaline condition [a]	*Streptomyces Auriofaciens*[a]	6.06 to 6.88[b]	4.85 to >6.2[b]	8.8, 21, to 49 days[a]

a[1]; b[2]; c[4]

3. Further details on the derivatization method, NAR quantification, and the HPLC equipment

3.1 Derivatization process

Before quantifying narasin concentrations in the equilibruim solutions, a derivatization procedure was carried out to improve the detectability of the NAR antibiotic by the UV detector.[5] In a first step, 100 µL of trichloroacetic acid was added to 700 µL of each adsorption/desorption sample, and the mixtures were vortexed (for approximatively 20 seconds). After a 10-min incubation period, a volume of 200 µL of 2,4-dinitrophenol acid was then added, and the samples were vortexed once again prior to be placed in an oven at 50°C for 20 min. Ultimately, NAR concentrations were measured using an Ultimate 3000 HPLC-UV device (model LPG 3400 SD, Thermo-Scientific, USA).

3.2. Description of the HPLC equipment

The HPLC device employed for the experimental measurements in this study was equiped with a quaternary pump and an auto-sampler. Chromatographic separations were conducted using a C18 analytical column (150 mm long; 4.6 mm internal diameter; 5 µm particle size) from Phenomenex (Madrid, Spain) and a pre-column (4 mm long; 3 mm internal diameter; 5 µm particle size), packed with the same material as the column.[6]

3.3 Quantification procedure

During these determinations, the samples were run with an isocratic method, with a single phase composed of methanol (88.5%), water (10%), and acetic acid (1.5%), with a flow rate set at 1 mL min^{-1}. Notably, the NAR chromatogram was resolved into three distinct peaks, with a retention time between 13.4 and 16.8 min and a total analysis time of 25 min, whose areas were summed up in a further step. The wavelength was 392 nm, using 200 µL as an injection volume. Chromatograms were then processed using Chromeleon software version 7 (Thermo Fisher Scientific, Madrid, Spain) and the areas of the three different peaks was summ up to quantify the total narasin. All these measurements were conducted at room temperature and in triplicate.

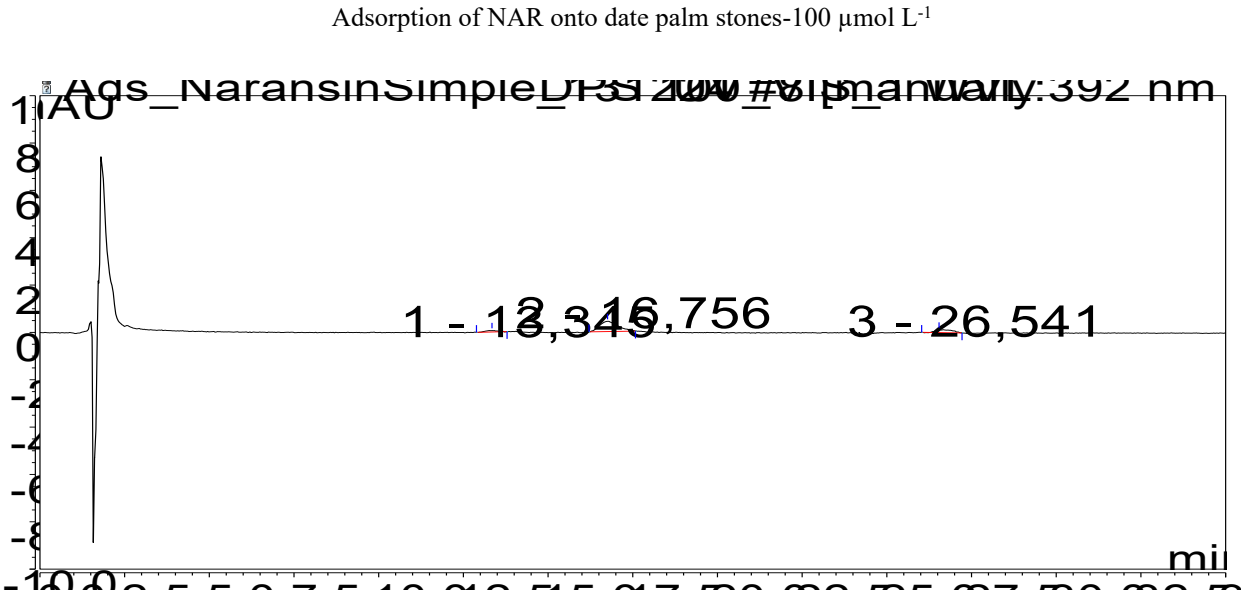

Figure S2. Selected HPLC chromatograms obtained for adsorption/desorption tests of narasin onto/from the bioadsorbents under study.

Adsorption of NAR onto pomegranate peel-100 µmol L^{-1}

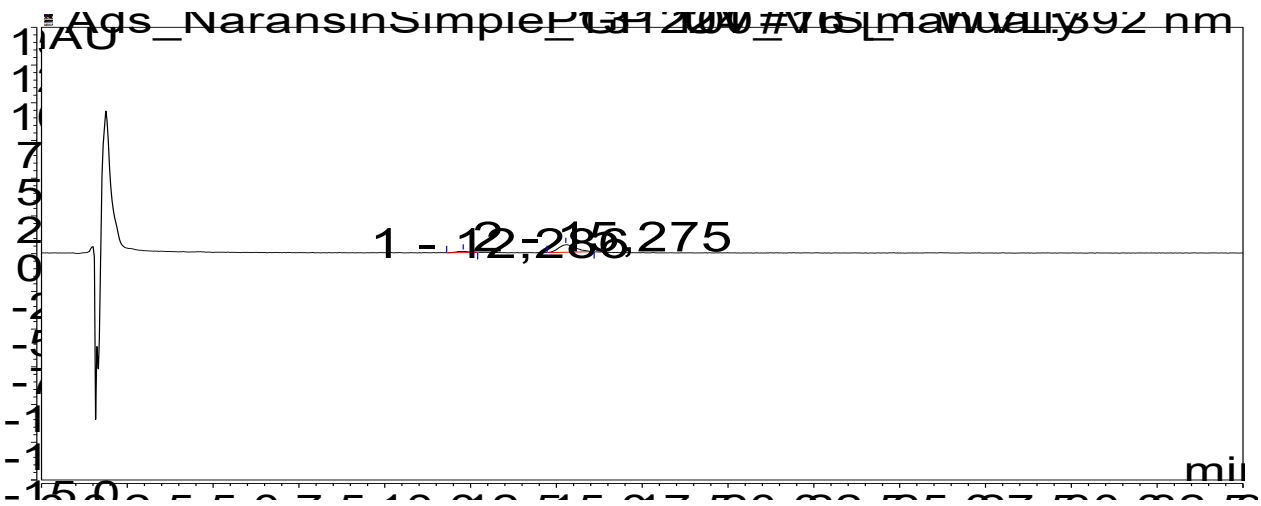

Desorption of NAR from cactus fiber-100 µmol L^{-1}

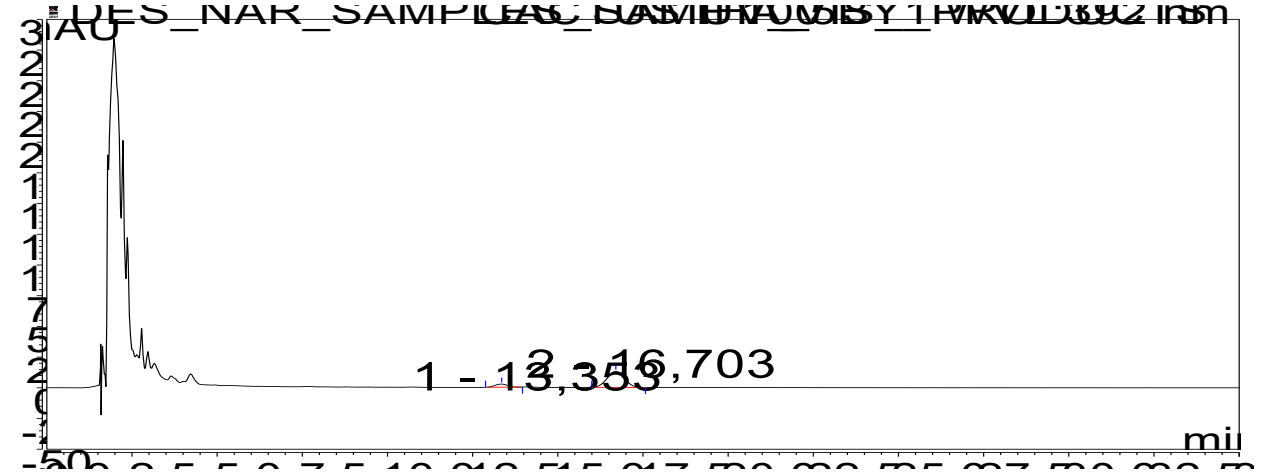

Figure S2. Continuation.

4. Statistical analysis and hysteresis calculations

To describe adsorption data, Freundlich (Eq. (1)), Langmuir (Eq. (2)), and the Linear model (Eq. (3)) were used:

$$q_a = K_F * C^n_{eq} \quad (1)$$

$$q_a = (q_{max}\, K_L * C_{eq}) / (1 + K_L * C_{eq}) \quad (2)$$

$$q_a = K_d * C_{eq} \quad (3)$$

Where q_a (µmol kg^{-1}) denotes the adsorbed amount of antibiotic per unit mass of the bio-adsorbent (difference between what is added and what remains in the equilibrium solution); C_{eq} (µmol L^{-1}) represents the concentration in the equilibrium solution of the antibiotic of study; K_F (L^n kg^{-1} μmol^{1-n}) is considered as the Freundlich constant related to the adsorption capacity; *n* (dimensionless) is a parameter related to the intensity of adsorption;[7] K_L (L µmol $^{-1}$) represents

the Langmuir constant associated with the adsorption energy; q_{max} (μmol kg^{-1}) is the Langmuir's maximum adsorption capacity, and K_d (L kg^{-1}) is the partition coefficient in the Linear model. Concerning the hysteresis index (*HI*), it was calculated as follows[8] (Eq. (4)):

$$HI = (q_a{}^D - q_a{}^S) / q_a{}^S \quad (4)$$

In this equation, $q_a{}^S$ (in μmol kg^{-1}) denotes the NAR concentrations adsorbed by the bio-adsorbent, and $q_a{}^D$ (in μmol kg^{-1}) is considered as the final NAR concentration after the desorption tests.

5. Characterization of the sorbent by-products

The physicochemical characterization of the studied bioadsorbents covered the following parameters: pH in water and in KCl (pH_w and pH_{KCl}), electric conductivity (EC, dS m^{-1}), moisture content (H, %), dry matter content (DM, as %), porosity (P, %), ash content (Ash, %), volatile matter content (VM, %), bulk density (BD, as g cm^{-3}), real density (RD, g cm^{-3}), swelling index (SI, %), organic matter content (OM, %), organic carbon content (OC, as %), exchangeable cations (Al, Ca, K, Mg, and Na, $cmol_c$ kg^{-1}), effective cation exchange capacity (eCEC, expressed in $cmol_c$ kg^{-1}), and lastely, particle size distribution (expressed as %).

Complementary details on the analytical procedures employed for the characterization of the investigated bioadsorbents were previsiouly documented. [9,10,11]

Additionally, the total non-crystalline Fe and Al contents (Fe_o and Al_o) were quantified by ammonium oxalate extraction at pH 3,[12] under stirring for 4 h in the dark; before centrifugation at 2000 rpm for 10 min and quantification, five drops of 0.25% superfloc were then added to the resulting extract, which was subsequently filtered, and the supernatant was diluted at a 1:5 ratio. The contents of Fe and Al bound to organic matter (Fe_{pir} and Al_{pir}) were also determined using sodium pyrophosphate extraction at pH 10 with a 1:100 solid-to-liquid ratio, under shaking for 16 h, after which the samples were diluted in half with distilled water.[13] Utimately, both fractions (Fe_o and Al_o / Fe_{pir} and Al_{pir}) were analyzed by atomic absorption spectrophotometry.

The determination of the surface area, pore volume, and pore size for all the bioadsorbents studied was performed using the Brunauer–Emmett–Teller (BET) method (Quantachrome Autosorb 1-MP).

Other elemental and structural analyses were condudted for the current work. Briefly, the elemental analysis of the biomaterials under study, encompassing carbon, oxygen, hydrogen, nitrogen, sulfur, and chloride (C, O, H, N, S, and Cl), was conducted according to AOAC official methods (AOAC 949.14 for C and H, AOAC 984.13 for N, AOAC 923.03 for S, and AOAC 926.03 for Cl). All analyses were performed on 1 g of material, with the resulting chemical parameters expressed on a dry matter basis, and carried out in triplicate for each sample.

Additionally, chemical composition of the studied bioadsorbents in terms of cellulose, hemicellulose, lignin, and pectin fractions was determined following standard protocols based on sequential acid/alkaline digestion and gravimetric determination.[14,15] Water content was measured gravimetrically after drying the samples in a ventilated oven at 105 °C for 48 h.

Finally, the surface functional groups of the bioadsorbents were determined by Boehm titration.[16,17] In this method, the determination of acidic and basic functionalities relies on their neutralization with bases and acids of increasing strength, according to their pK_a values. Specifically, carboxylic groups (the strongest) are neutralized by $NaHCO_3$ (pK_a = 6.4), while NaOH (pK_a = 15.7) neutralizes phenolic groups. In turn, NaOEt (pK_a = 20.6) reacts with the basic groups,including carbonyl-containing groups;[18] however, nowadays HCl is increasingly used for the neutralization of basic groups.[18] The results were expressed as milliequivalents per gram of dry sample.

5.1 Physicochemical parameters

Table S3 lists the main characteristics of the fourteen studied bioadsorbents.

According to Table S3, the tested bio-materials exhibited marked variability in their physicochemical properties. Briefly, OM contents were notecably elevated in AS (68.4%) and OP (65.9%), followed by DPS, EB, and AB (49.21-56.3%), whereas the remaining adsorbents displayed considerably lower levels (17-41.5%). A similar trend was observed for organic carbon (OC%) contents in the aforementioned bioadsorbents, ranging from 23.62% (AB) to 32.8% (AS), as was the case for Ca_e cations, which reached up to 12.5 cmolc kg^{-1} for AS and declined to 7.44 cmolc kg^{-1} in AB, with notably high Ca_e levels also recorded in PS and AF (7.8 and 6.74 cmolc kg^{-1}, respectively) (Table S3).

Furthermore, AS, OP, DPS, AB, EB, PS, and AF had higher Al_e levels (0.11-1.4 cmolc kg^{-1}) and greater eCEC scores (13.97-26.7 cmolc kg^{-1}), compared to the lower ranges noted for the other bioadsorbents (Al_e: 0.04-0.4 cmolc kg^{-1}; eCEC: 8.55-13.7 cmolc kg^{-1}). Moderately elevated eCEC values were also marked in the case of POF, CC, and ZOB (11.4-12.38 cmolc kg^{-1}), exceeding those observed for CF, PF, and CGs (8.55-10.4 cmolc kg^{-1}) (Table S3).

As shown in Table S3, AF, AS, OP, and DPS displayed the highest values of BET surface area (oscillating between 1.064 and 2.683 m^2 g^{-1}) and pore volume (between 0.056–0.083 cm^3 g^{-1}), with AF exhibiting the greatest values. Conversely, PF, AB, and EB presented lower surface areas (ranging from 0.468 to 0.934 m^2 g^{-1}) and pore volumes (between 0.031-0.047 cm^3 g^{-1}), while maintaining higher pore sizes relative to the former samples; these values are considered moderate compared to CF, POF, ZOB, PGP, PS, CGs, and CC, although they characterized the largest pore sizes (between 16.45–23.21 nm) among the 14 bioadsorbents under study (Table S3).

Lastely, particle size distribution revealed that AS, OP, DPS, PS, and the three natural barks (AB, EB, and ZOB) were predominantly composed of particles ranging from 50-75 μm, similar to those observed in PGP and the four natural fibers (mostly 75-100 μm), whereas both raw and calcined coffee grounds exhibited finer particles (<200 μm) (Table S3).

All measurements and adsorption-desorption experiments were performed in triplicate (n = 3).

Table S3. Chemical characteristics of the bioadsorbents, with average values (n = 3) and coefficients of variation always <5%.

	Bioadsorbents													
Parameters	**AF**	**CF**	**PF**	**POF**	**AB**	**EB**	**ZOB**	**OP**	**PGP**	**PS**	**AS**	**DPS**	**CGs**	**CC**
pH_w	5.1	7.4	5.5	5.5	4.9	5.4	5.7	4.6	3.7	4.2	5.2	5.4	5.8	6.0
pH_{KCl}	4.7	7.6	6.9	5.3	4.2	5.1	4.8	3.5	3.9	4.4	5.0	5.1	6.3	5.6
pH_{PZC}	6.6	6.2	4.3	5.6	7.1	7.4	5.8	7.1	3.9	6.5	7.3	7.5	5.2	6.3
EC (dS m^{-1})	21	204	818	2.3	19.7	4.2	5.9	4.9	1.8	2.6	5.6	3.8	1.4	1.8
H % (%)	9.3	6.2	5.4	4.8	10.7	11.5	7.0	13.4	6.6	8.7	14.2	10. 5	4.3	1.2
DM (%)	90.7	93.8	94.6	95.2	89.3	88.5	93.0	86.7	93.3	91.2	85.3	89.4	95.6	98.8
P (%)	86.6	48.0	41.6	24..3	62.8	65.7	57.5	40.3	26.5	28.4	43.8	37.9	17.6	20.4
Ash (%)	2.45	3.34	4.36	2.75	1.22	1.42	1.91	4.3	6.2	5.4	0.3	1.8	6.7	1.9
VM (%)	97.55	96.66	95.64	97.25	98.58	98.58	98.0	95.7	93.8	94.6	99.7	95.2	93.3	98.1
BD (g cm^{-3})	1.28	0.96	0.81	0.8	1.42	1.53	1.1	0.7	0.4	0.2	1.0	1.3	0.4	0.6
RD (g cm^{-3})	1.65	1.23	1.14	0.9	1.86	1.97	1.43	0.9	0.5	0.4	1.2	1.5	0.6	0.7
SI (%)	2.56	1.43	1.08	2.1	2.82	2.96	1.84	9.4	5.5	6.5	9.1	6.8	4.2	1.7
OM (%)	40.72	21.76	18.84	20.67	49.21	50.25	29.8	65.9	36.3	41.5	68.4	56.3	30.3	17.0
OC% (%)	19.54	10.44	9.04	18.56	23.62	24.12	14.3	31.6	17.4	19.9	32.8	27.0	14.5	8.16
Al_e ($cmol_c$ kg^{-1})	0.11	0.05	0.05	0.09	0.18	0.11	0.09	1.2	0.2	0.4	1.4	0.6	0.1	0.04
Ca_e ($cmol_c$ kg^{-1})	6.74	2.04	1.97	5.63	7.44	7.98	4.22	10.7	5.9	7.8	12.5	8.5	2.5	2.71
K_e ($cmol_c$ kg^{-1})	2.22	3.04	2.96	2.13	2.02	2.07	2.79	8.24	3.9	4.8	9.1	6.5	3.2	4.02
Mg_e ($cmol_c$ kg^{-1})	1.57	3.06	2.99	2.04	1.03	0.86	2.81	1.5	3.5	2.8	1.2	2.6	4.4	1.32
Na_e ($cmol_c$ kg^{-1})	2.32	1.05	0.96	0.73	3.77	4.04	1.12	1.4	0.2	0.8	2.5	1.1	0.1	1.0
eCEC ($cmol_c$ kg^{-1})	13.97	9.26	8.55	12.38	14.45	15.08	11.4	23.2	13.7	16.6	26.7	19.3	10.4	12.1
Al_o (mg kg^{-1})	520	110	50	110	525	545	190	1375	500	515	3010	695	245	35
Fe_o (mg kg^{-1})	650	145	75	110	660	800	220	2695	650	655	3265	1265	635	50
Al_{pir} (mg kg^{-1})	115	75	60	60	225	485	75	550	90	145	870	530	90	20
Fe_{pir} (mg kg^{-1})	80	35	30	30	270	280	70	565	75	80	605	475	55	15
S_{BET} (m^2 g^{-1})	2.683	0.302	0.934	0.271	0.473	0.468	0.353	1.145	0.356	0.308	1.314	1.064	0.103	0.214
P.V (cm^3 g^{-1})	0.083	0.026	0.047	0.019	0.033	0.031	0.024	0.061	0.020	0.023	0.067	0.056	0.010	0.016
P.S (nm)	12.67	16.45	10.670	20.41	18.11	18.64	15.23	9.43	18.34	18.79	8.22	9.81	23.21	20.73
Particle size (%)														
0.075-0.1 mm	86.17	52.28	66.71	93.2	26.14	31.30	39.0	11.6	60.8	32.6	10.4	16.3	--	--
0.05-0.075 mm	11.68	30.61	15.77	5.67	68.43	65.45	53.0	79.4	29.7	58.8	85.7	70.0	3.4	1.3
0.05-0.02 mm	2.15	10.73	13.47	1.14	4.16	3 .25	6.78	5.5	9.5	--	2.1	7.8	20.1	11.1
< 0.02 mm	--	6.38	4.05	--	1.27	--	1.20	2.1	--	8.6	1.8	5.9	76.5	87.6

EC: electrical conductivity; H%: Moisture content; DM: Dry matter content; P: Porosity; Ash: Ash content; VM: Volatile matter content; BD: Bulk density; RD: Real density; SI: Swelling Index; OM: organic matter content; OC%: Organic carbon content; X_e: exchangeable cations (Al, Ca, K, Mg, and Na); eCEC: effective cation exchange capacity; Al_o, Fe_o: non-crystalline Al and Fe (extracted with ammonium oxalate); Al_{pir}, Fe_{pir}: Al and Fe extracted with sodium pyrophosphate; S_{BET}: BET surface area; P.V: pore volume; P.S: pore size.

5.2 Analysis of functional groups in the bioadsorbents

Fig. S3 shows the relative contents of surface functional groups for the fourteen by-products under investigation.

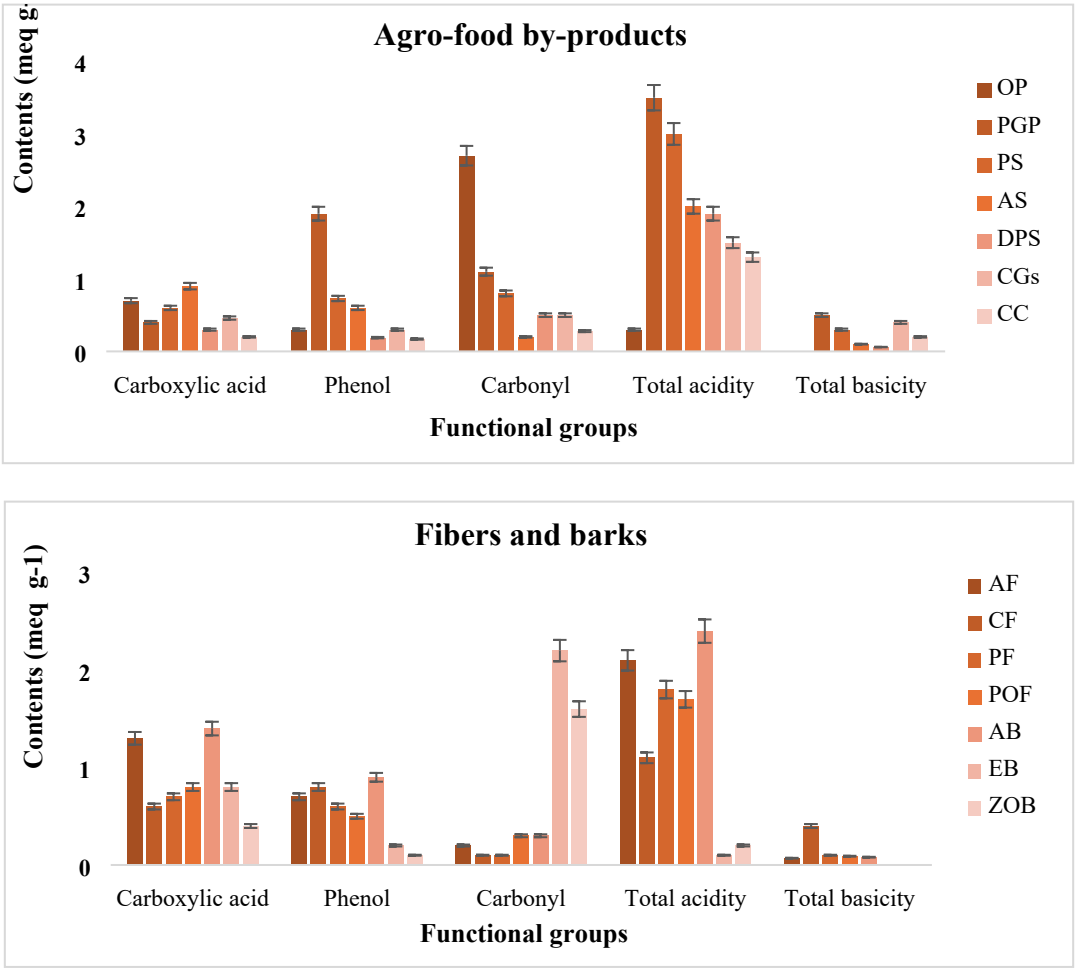

Figure S3. Relative contents of surface functional groups of the studied bioadsorbents. Average values (n = 3), with coefficients of variation always <5%, and error bars represent the standard deviation.

6. Adsorption results expressed as percentage

Fig. S4 presents the adsorption curves, illustring the adsorption capacity of each adsorbent by-product expressed as a percentage.

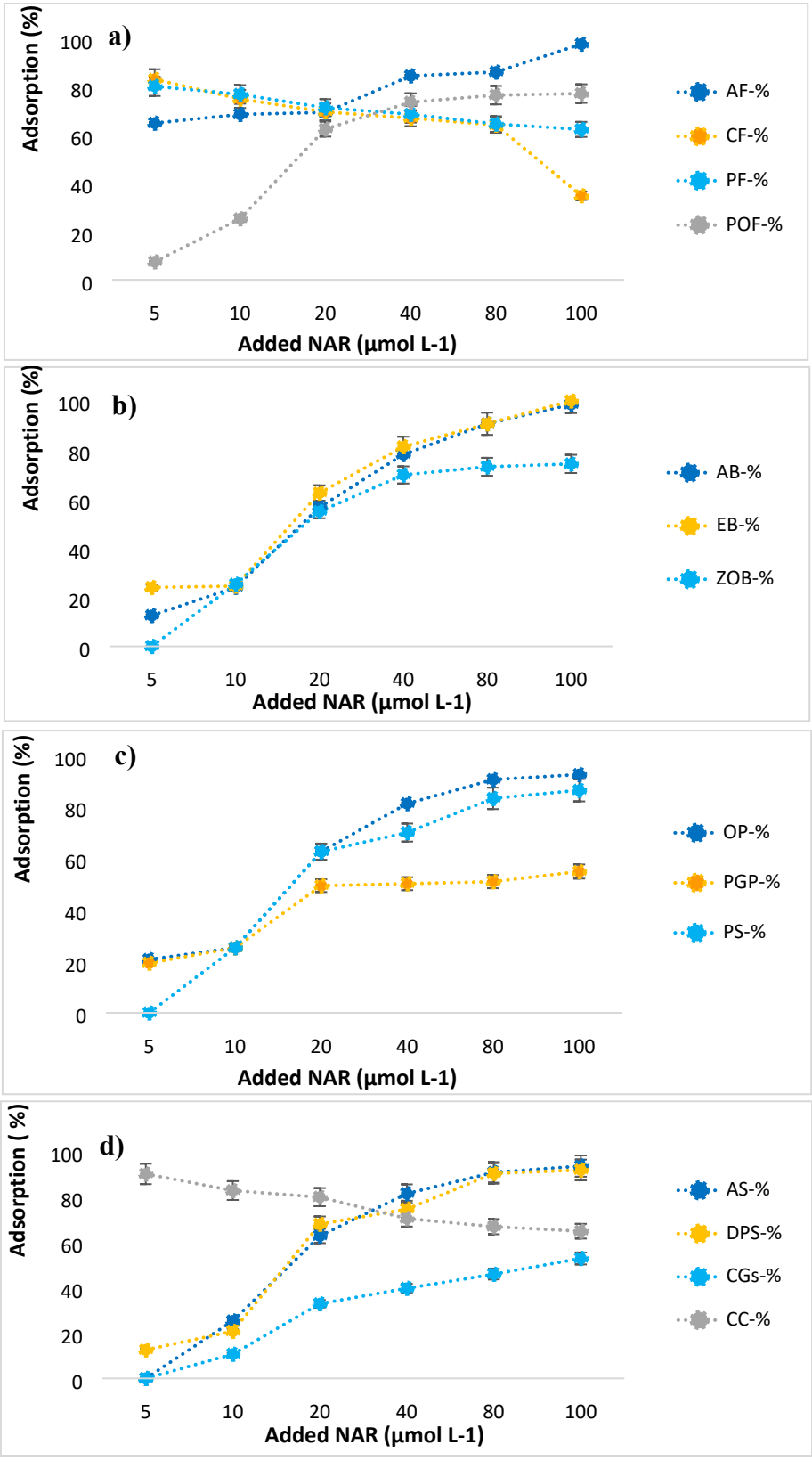

Figure S4. Adsorption curves of narasin (NAR) (expressed as %) for the natural fibers (a), barks (b), and the agro-food by-products (c,d), as a function of the antibiotic concentration added (µmol L^{-1}). Average values (n = 3), with coefficients of variation always <5%, and error bars represent the standard deviation.

7. Relationship between adsorption and by-product characteristics / pH in the equilibrium

The relationship between the adsorption efficiency and the main physicochemical properties was evaluated using Pearson correlation tests, as presented in Table S4.

The removal yield of narasin was found to vary primarily depending on the type of by-product used. In this context, Fig. S5 illustrates the variation in mean adsorption as a function of (a) the type of adsorbent biomaterial and (b) the pH observed in the equilibrium solutions.

Table S4. Pearson's r correlations between narasin (NAR) adsorption values and main bio-adsorbent characteristics known to affect the adsorption process. The abbreviations of the bioadsorbents' characteristics retain the same meaning as in Table S2.

Parameters	Correlation Coefficient (r)	Significance Level (*p*)
pH_w	-0.371	--
pH_{KCl}	-0.717	0.01
pH_{PZC}	0.211	--
EC (	0.189	--
H% (%)	0.619	0.01
DM (%)	0.619	0.01
P (%)	0.461	0.05
Ash (%)	-0.478	0.05
VM (%)	-0.478	--
SI (%)	0.363	--
BD (g cm^{-3})	0.335	--
RD (g cm^{-3})	0.321	--
OM (%)	0.639	0.01
OC% (%)	0.639	0.01
Al_e ($cmol_c$ kg^{-1})	0.209	--
Ca_e ($cmol_c$ kg^{-1})	0.665	0.01
K_e ($cmol_c$ kg^{-1})	0.311	--
Mg_e ($cmol_c$ kg^{-1})	-0.032	--
Na_e ($cmol_c$ kg^{-1})	0.510	0.05
eCEC ($cmol_c$ kg^{-1})	0.378	0.05

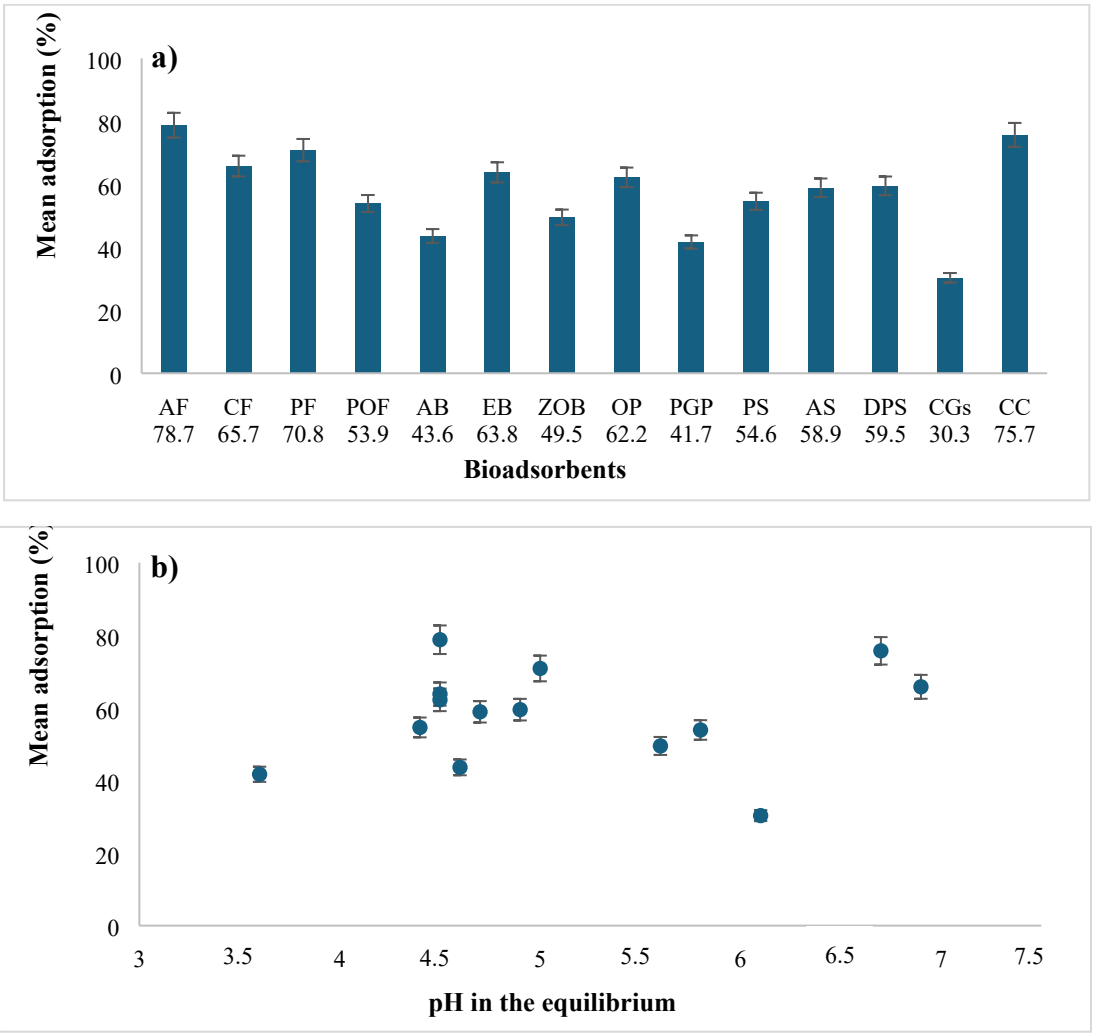

Figure S5. Variation of mean adsorption (%) as a fuction of (a) the type of adsorbent used and (b) the mean pH levels detected in the equilibrium solutions (b). Average values (n = 3), with coefficients of variation always <5%, and error bars represent the standard deviation.

Additionally, Table S5 shows the variation of pH values in the aqueous solutions of the antibiotic and the by-products under investigation.

Table S5. Variation of pH values in aqueous solutions containing NAR and the adsorbent by-products studied.

	By-products													
$pH_{ads\ (CaCl2)}$	**AF**	**CF**	**PF**	**POF**	**AB**	**EB**	**ZOB**	**OP**	**PGP**	**PS**	**AS**	**DPS**	**CGs**	**CC**
Min	4.1	6.1	4.6	5.6	4.3	4.0	5.3	3.9	3.0	3.8	3.8	4.2	5.5	6.4
Max	4.9	7.7	5.4	6.0	4.9	4.9	5.9	5.1	4.2	5.0	5.6	5.6	6.7	7.0
Mean	4.5	6.9	5.0	5.8	4.6	4.5	5.6	4.5	3.6	4.4	4.7	4.9	6.1	6.7

pH_{ads} : pH of the aqueous solutions containing NAR and different bioadsorbents during the adsorption process. Mean values based on three repetitions, with coefficients of variation always below 5.

8. Effect of pH on adsorption process

8.1 Variation of sorption percentage as a function of solution pH

In this research, the effect of pH on NAR retention was elucidiated using the six most efficient samples (Fig. S6).

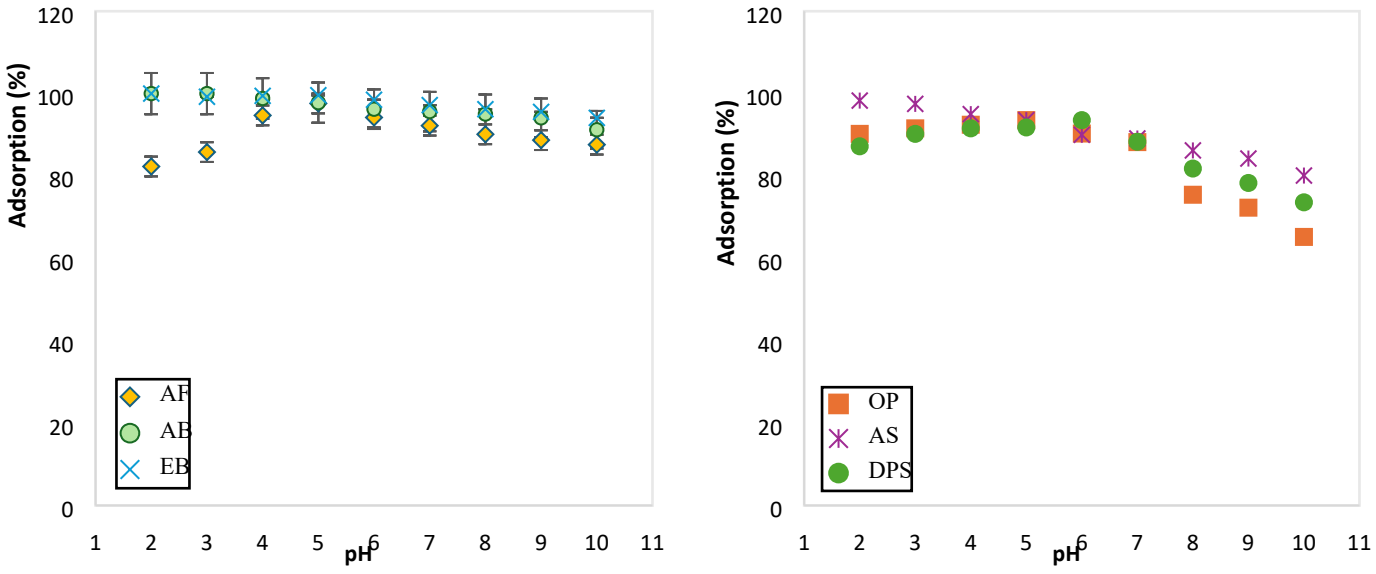

Figure S6. Adsorption of narasin on the six most adsorptive by-products (AF, AB, EB, OP, AS, and DPS) as a function of solution pH. Average values (n = 3), with coefficients of variation always <5%, and error bars represent the standard deviation.

8.2 Futher detail on the protonation/deprotonation of NAR as a function of solution pH

Regarding the electrical charge of NAR, some authors have used a pK_a value of 7.9, calculated in organic solvents or in solvent/water mixtures (80 % dimethylformamide),[19] to discuss its adsorption in soils.[2,21,1] However, for studies dealing with NAR removal from aqueous solutions, the pK_a value of 4.4 calculated in water by Bak et al. (2013)[4] using Marvinsketch™ (Table S2, Supplementary Material) is more commonly applied. Accordingly, this study considers a pK_a of ~4.4, indicating that NAR is protonated (positively charged) in an acid medium.

9. Adsorption modeling and Schatchard analysis

9.1 Adsorption modeling

Fig. S7 shows the adsorption curves representing the experimental results obtained in this research for the set of antibiotics and bioadsorbents tested.

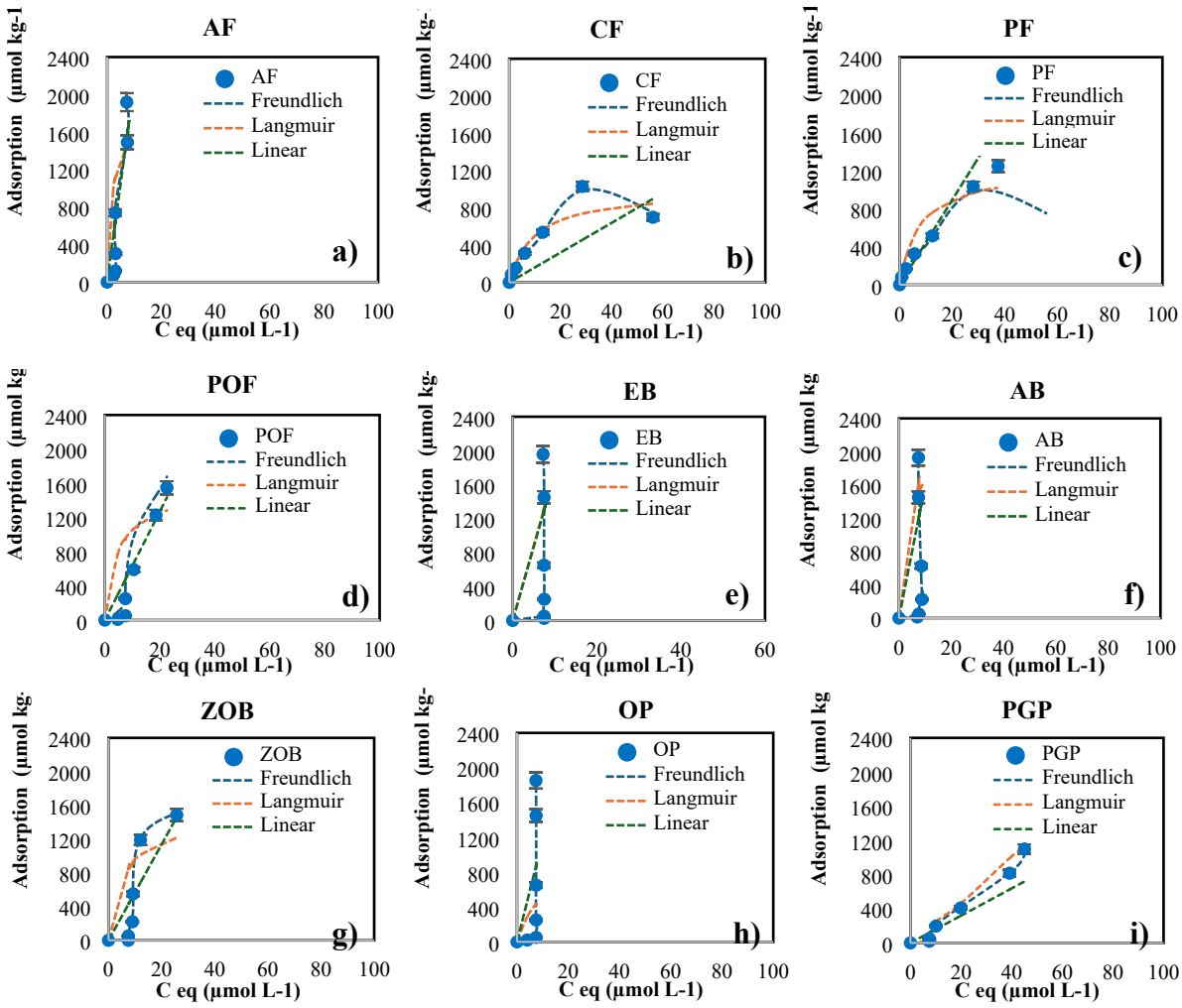

Figure S7. Adsorption curves for NAR onto natural fibers (a–d) and barks (e-g), as well as agro-food by-proucts (h-n). Average values (n = 3), with coefficients of variation always <5%, and error bars represent the standard deviation.

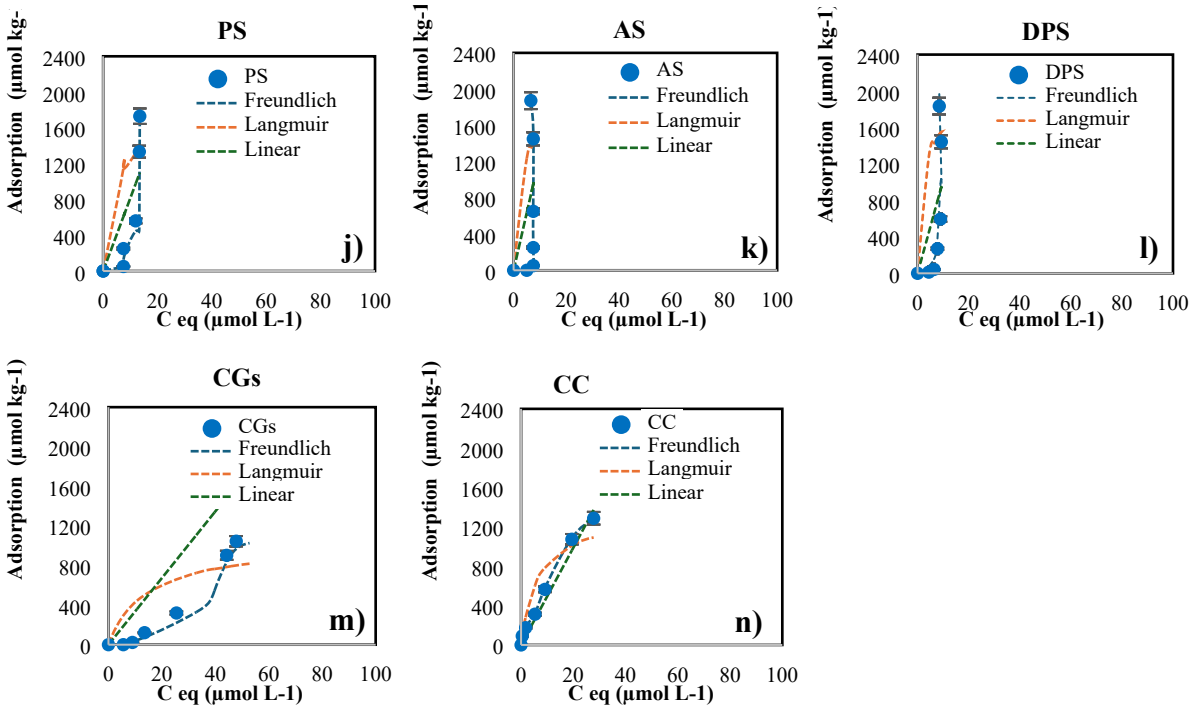

Figure S7. Continuation.

In addition, Table S6 summarizes the Pearson correlation coefficients (r) obtained between the Freundlich parameters (K_F and *n*) and the main characteristics of the studied by-products, providing insight into the influence of these parameters on adsorption behavior.

Table S6. Pearson's correlation coefficient (r) obtained from correlations between the Freundlich parameters (K_F and *n* value) and the key by-product characteristics. K_F: Freundlich adsorption coefficient; and *n*: Freundlich linearity index.

Adsorbent parameter	K_F	*n*
pH_w	0.075	0.012
pH_{KCl}	-0.065	-0.043
pH_{PZC}	0.123	0.092
EC	0.109	0.067
H%	0.703*	0.632*
DM	0.703*	0.632*
OM	0.534*	0.543*
OC%	0.534*	0.543*
P	0.584*	0.487*
Ash	-0.830**	-0.579**
VM	-0.830**	-0.579**
SI	0.117	0.110
BD	0.625*	0.432*
RD	0.562*	0.465*
OM	0.534*	0.512*
OC%	0.534*	0.512*
Al_e	0.247	0.147
Ca_e	0.525*	0.493*
K_e	0.306	0.233
Mg_e	-0.655*	-0.612*
Na_e	0.741**	0.657**
eCEC	0.349	0.323

* Significant at a P-value of 0.05. ** Significant at a P-value of 0.01.

9.2 Schatchard plots

Scatchard plots, obtained by plotting q_a values (adsorbed amounts of NAR, in μmol kg^{-1}) versus the q_a / C_{eq} ratio (C_{eq} : equilibrium concentration, in μmol L^{-1}) for all tested sorbent by-products,

are presntend in Fig. S8, providing insight into the binding affinity and capacity of each material.

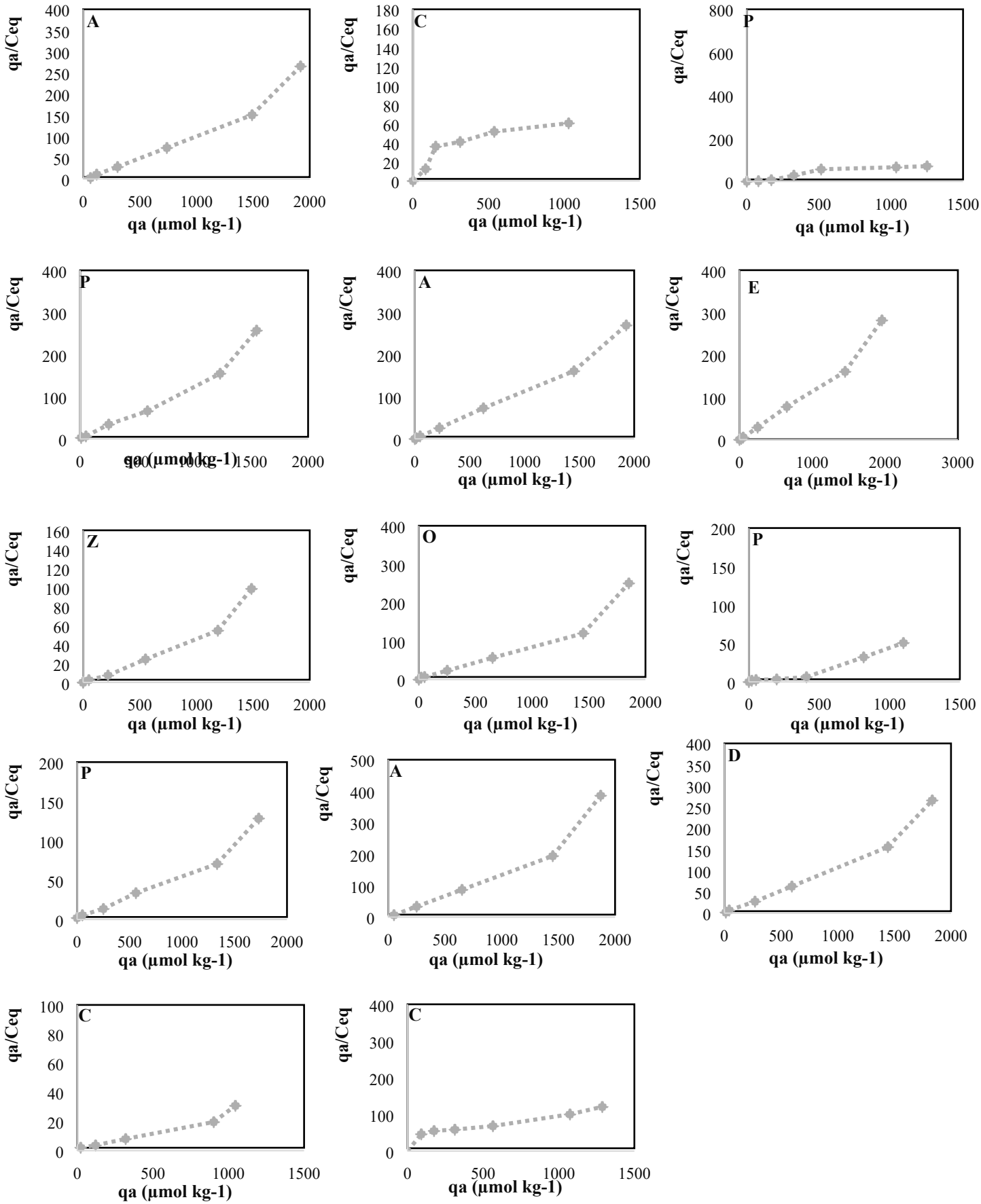

Figure S8. Scachard plots derived for sorption data obtained for the bioadsorbents tested.

10. Further details on FTIR analysis

10.1 Infra-red (IR) bands

Tables S7a and S7b lists the wavenumbers (expressed in cm^{-1}) corresponding to the main characteristic IR peaks detected in each analyzed by-product.

Table S7a. The main characteristic IR bands (wavenumbers in cm^{-1}) of the investigated fibers and barks before and after NAR adsorption.

Number	Raw fibers and barks							Fibers and barks + 100 µmol L^{-1} of NAR						
	AF	**CF**	**PF**	**POF**	**AB**	**EB**	**ZOB**	**AF**	**CF**	**PF**	**POF**	**AB**	**EB**	**ZOB**
0	3324	3320	3320	3320	3334	3334	3063-3334	3319.2	3314.5	3325.7	3335.1	3333.4	3322.6	3320.4
1	2917	2918	2916	2917	2919	--	2923	2917	--	--	2918	2919	2918	2917
2	2849	--	--	--	--	--	--	--	--	--	--	2850	2849	--
3	--	--	--	1726	--	--	--	--	--	--	1729	--	--	--
4	1637	1634	1606	1622	1621	1625	1625	1637	1636	1636	1606	1610	1616	1640
5	--	1506	1513	1501	1517	--	--	1505	1506	1512	1513	1518	1516	--
6	1463	1458	--	1455	1446	1449	1447	1462	1458	--	--	1445	1446	1462-1427
7	1421	1424	1421	1421	--	--	--	1421	1424	1421	1421	--	--	--
8	1319-1358	1316-1371	1320-1374	1318-1371	1317	1316-1364	1316-1363	1369	1370	1371	1374	--	--	1370
9	1244	1240	1244	1235	--	--	1239	1319	1318	1317	1320	1316	1316	1316
10	1161	1158	1156	1157	--	--	--	1241	1243	1246	1244	1283-1208	1220	1245
11	1031	1033	1034	1035	1031	1031	1032	--	--	--	--	1100	1099	1161-1105
12	--	--	--	--	--	--	--	1032	1033	1032	1034	1016	1017	1016
13	--	--	--	800.1-896.5	--	--	883.3	895.9	--	--	874.4	--	--	--
14	--	--	--	--	--	--	--	--	--	--	--	--	--	--
15	532.7	525.9	530.4	--	529.6	529.6	600	556.6	555.4	--	--	504.6	533	--

Table S7b. The main characteristic IR bands (wavenumbers in cm^{-1}) of the agro-food by-products studied before and after NAR sorption.

Number	Raw agro-food by-products							Agro-food by-products + 100 µmol L^{-1} of NAR						
	OP	**PGP**	**PS**	**AS**	**DPS**	**CGs**	**CC**	**OP**	**PGP**	**PS**	**AS**	**DPS**	**CGs**	**CC**
0	3350	3292.2	3350	3350	3350	3350	3319	3291.7	3324.2	3307.35	3288.6	3294.1	3334.5	3301.6
1	2924	2985	2985	2926	2926	2923	2921	2954	2934	2918	2918	2919	2922	2917
2	2876	--	2876	--	2870	2853	2851	--	--	2850	2850	2850	2850	2852
3	1744	1713.5	1740	1733	1745	1743	--	1730	--	1703	1726	1727	1742	1726
4	1649	1607.21	1600	--	1640	1652	1638	1643	1617	1632	1613	1614	1639	1622
5	1580	--	--	1585	--	1552	1541	1520	1514	--	1519	1519	1540	1504
6	1455	1443.81	1440-1477	1462-1482	1444-1477	1450-1464	--	1421	1445	1420	1442	1442	1455	1421-1455
7	1430	--	1407	--	--	--	--	1320-1368	1328	1317-1371	1372	1371	1311-1376	1318-1371
8	1370	1322.65	1375	1375	1375	1374	1308-1370	1242-1276	1231	1243	1248	1247	1245	1235
9	--	--	1279	1222	1279	1260	1246	1103-1152	1105.4	1103-1158	1104-1158	1150	1157	--
10	1260	1181.61	--	1150	1150	1150	1148	1097	--	--	--	--	--	--
11	1030	1029.18	1026	1030	1080	1026	1029	1015	1015	1015	1018	1018	1023-1060	1031
12	--	985	943	--	--	900	--	964.8	922.3	961.6	--	--	--	--
13	870	875.7	--	820-870	--	807-850	--	--	--	--	821	--	871	--
14	750 690	748.3 --	750 --	748 690	--	--	--	--	--	--	--			
15	--	--	--	--	--	--	--	--	--	--	533.6	529	533	--

10.2 Descriptive IR features of the studied bioadsorbents with NAR

Details on other preferential peaks, together with minor bands (≤ 985 cm^{-1}) observed in the IR spectra of biomaterials object of this study exposed to 100 µmol L^{-1} of NAR for 48 h of contact time (after adsorption) (Fig. 2 ; Tables S7a and 7b) are presented below.

The pivotal role of lignin (or pectin) in retaining the antibiotic molecules on some of the studied bioadsorbents is evidenced by the disappearence of the peaks at 1726-1745 cm^{-1}, assigned to the carbonyl groups (such as esters in lignin and/or pectin), from the IR spectrum of PGP after NAR adsorption, while they solely shifted from their original wavenumbers in case of the remaining bio-materials where they are present[22] (Tables S7a and 7b; Fig. 2).

Moreover, the shifts in 1421-1482 cm^{-1} bands corresponding to EB, ZOB, OP, PS, AS, and DPS, along with the absence of the peaks within the 1463-1482 cm^{-1} range in the IR spectra of PS and AS, as well as DSP, and their subsequent appearance in the IR spectrum of CC sample after adsorption, strongly indicate the involvement of carboxylic acids in sorption process, either in their protonated (R–COOH) form ($pH < pk_a$) or deprotonated (carboxylate ion ($R–COO^-$)) form ($pH > pk_a$) depending the pH of the solution. Moreover, the formation of hydrogen bonds among carboxyl groups (O- CO) and amino-groups (N-H) can also change peak values mentioned above.

Concerning the peaks observed at 1370-1375 cm^{-1} range, they are split into two smaller peaks after adsorption, in case of OP, PS, and CGs, appearing in the ranges 1368-1376 cm^{-1} and 1311-1320 cm^{-1}. This splitting may be associated with new binding sites, while the latter band already existed in fibers, barks, and calcined coffee grounds before NAR being adsorbed onto their surfaces (Tables S7a and 7Sb; Fig. 2).

In the same way, the acetyl group peak (lignin, at 1222-1279 cm^{-1}) fluctuated during adsorption, as it presents with higher wavenumbers for fibers and barks (except for CF) and lower wavenumbers for agro-food bioadsorbents (except for OP and PS).

According to the literature, the chlorogenic acids and Olefin groups ($\nu(–CH_2)$) abundant in CGs with their characteristic absorption bands typically appearing within the 1000–1450 cm^{-1} [23] and 807-850 cm^{-1} (which shifted to 871 cm^{-1} after adsorption) ranges, respectively, may hindered its capacity to retain NAR via weak hydrophobic and π-π interactions. Analogously, the absence of these components in CC sample may contribute to their relatively high sorption efficiency compared to CGs. The absence of these components in the CC sample may account for its relatively higher sorption efficiency in comparison with CGs.

Althought the IR peaks observed at wavenumbers lower than or equal to 985 cm^{-1} exhibit low intensities, may suggest the lesser relevance of the associated functional groups as major contributors in NAR adsorption onto the biomaterials under investigation; however, their shifting or displacement during adsorption alows us to gain deeper insight into the chemical and/or physical interactions that stand out as mechanisms faciltaing the adsorptin of NAR molecules onto the studied bioadsorbents: i) the disappearance of peaks in the 690-750 cm^{-1} range from the IR spectra of OP and PGP, as well as PS, and the peaks in the 870-896.5 cm^{-1} region from the IR spectra of ZOB, OP, PGP and AS, which correspond to out-of-plane C-H bending vibrations in the aromatic rings of lignin, suggests their involvement in hydrogen bonding or π-π stacking interactions with NAR, thus, resulting in modifications of the bending vibrations; ii) the complete absence of the peaks at 690-750 cm^{-1} area for the fibers and the

barks, except for zean oak batk, both before or after adsorption, suggests that hydrogen bonding and π-π stacking interactions play a lesser role in NAR adsorption onto these bio-adsorbent by-products; iii) the appearance of low-intensity peaks at 922.3-985 cm^{-1} (exclusively noted for PGP and PS before and after adsorption and for OP after adsorption) with fluctuated wavenumbers could reflect the existence of various types of polysaccharides in these materials[24,25,26], which contain functional groups like hydroxyl groups (-OH) that facilitate their interacts with NAR molecules via hydrogen bonds; and finally iv) the shifting of the wavenumbers at 525.9-600 cm^{-1} after adsorption may indicate the formation of metal-oxygen bonds during the adsorption process or the formation of complexes between the antibiotic and Na^+ cations.[27]

11. Solid-state ^{13}C NMR analysis

Fig. S9 displays the solid-state ^{13}C NMR spectra of the nine selected samples.

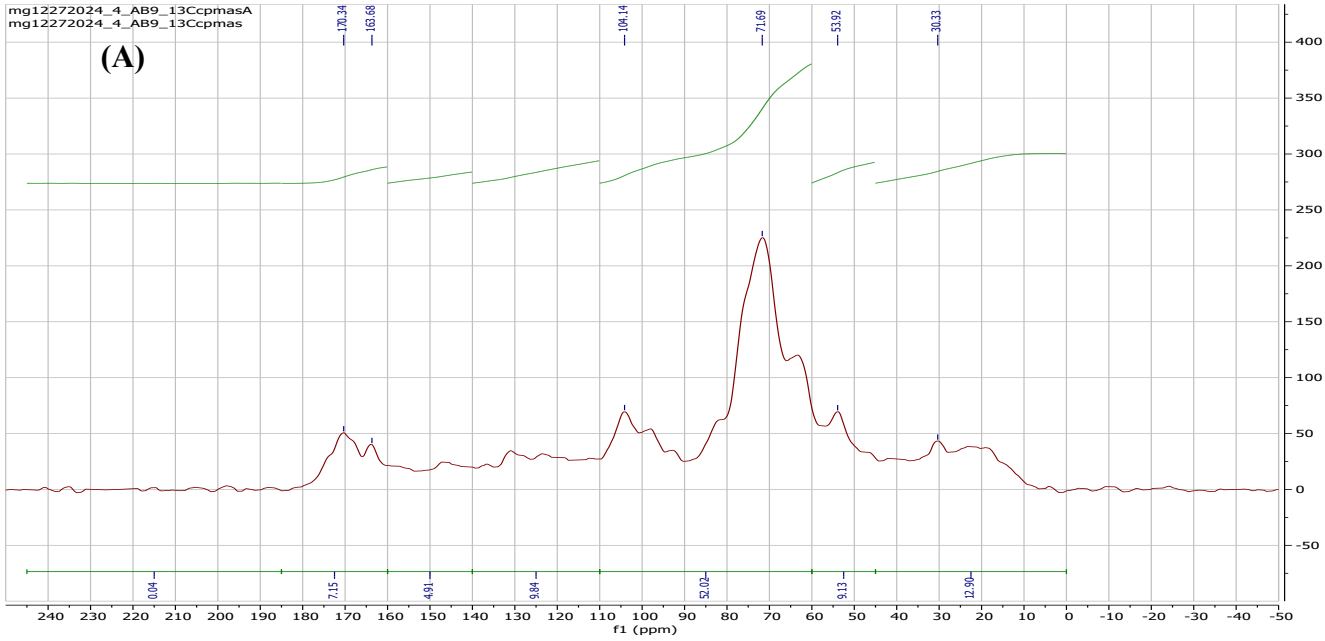

Figure S9. Solid-state ^{13}C NMR spectra of the nine selected adsorbent by-products. A): alfa fiber; B) acacia bark; C) eucalyptus barks; D) orange peel; E) almond shell; F) date palm stones; G) zean oak bark; H) pomegranate peel; and I) coffee grounds.

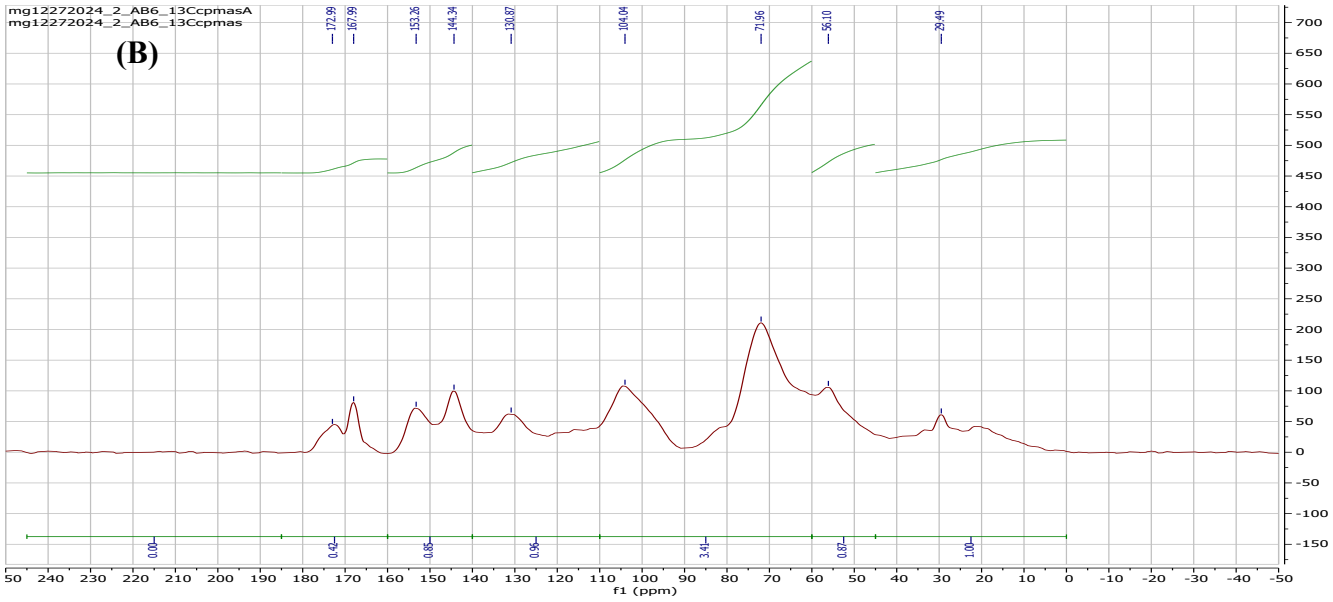
mg12272024_2_AB6_13CcpmasA
mg12272024_2_AB6_13Ccpmas
(B)
172.99
167.99
153.26
144.34
130.87
104.04
71.96
56.10
29.49
0.00
0.45
0.85
0.96
3.41
0.87
1.00
f1 (ppm)

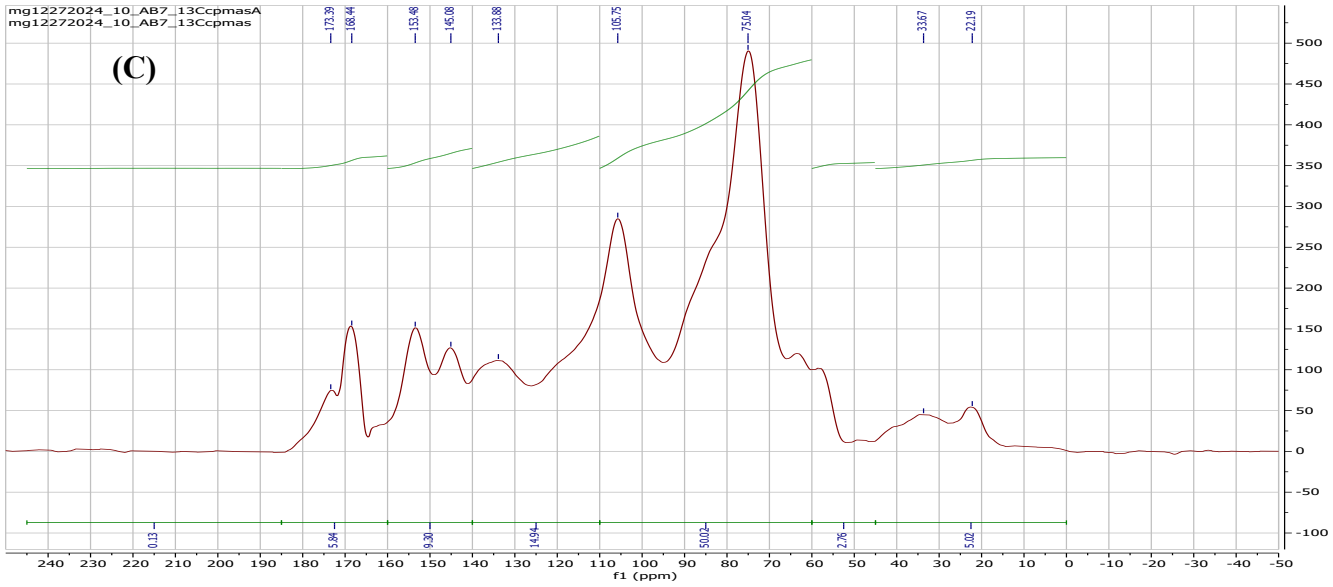
mg12272024_10_AB7_13CcpmasA
mg12272024_10_AB7_13Ccpmas
(C)
173.39
168.44
153.48
145.08
133.88
105.75
75.04
33.67
22.19
0.13
5.84
9.30
14.94
50.02
2.76
5.02
f1 (ppm)

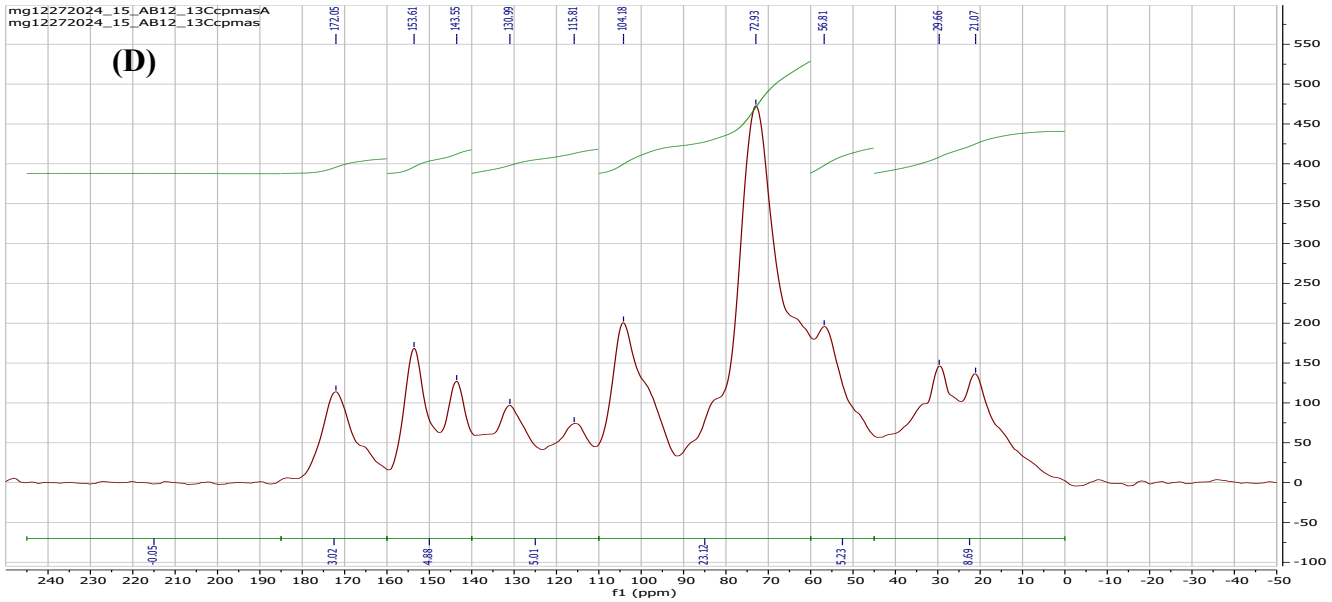

Figure S9. Continuation.

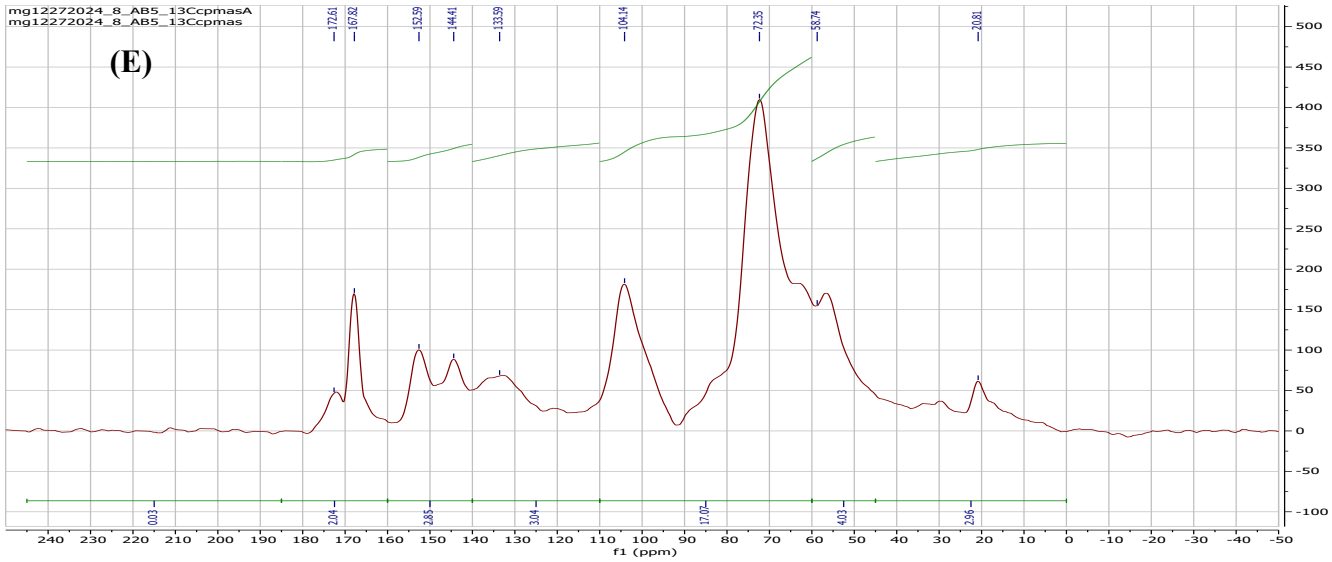

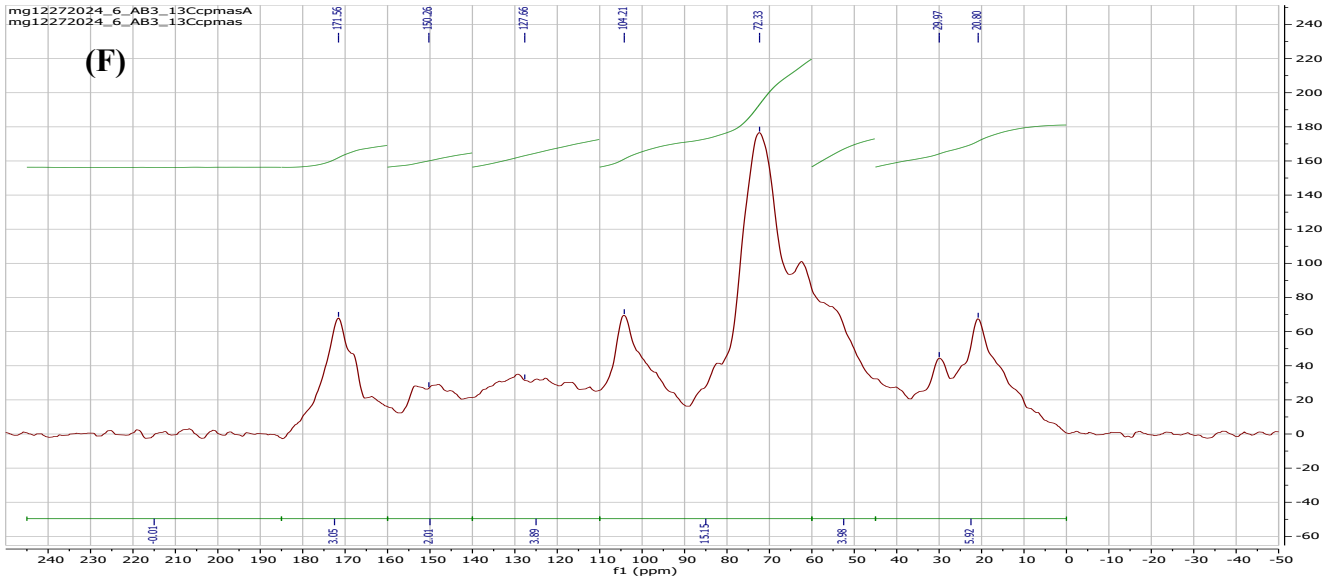

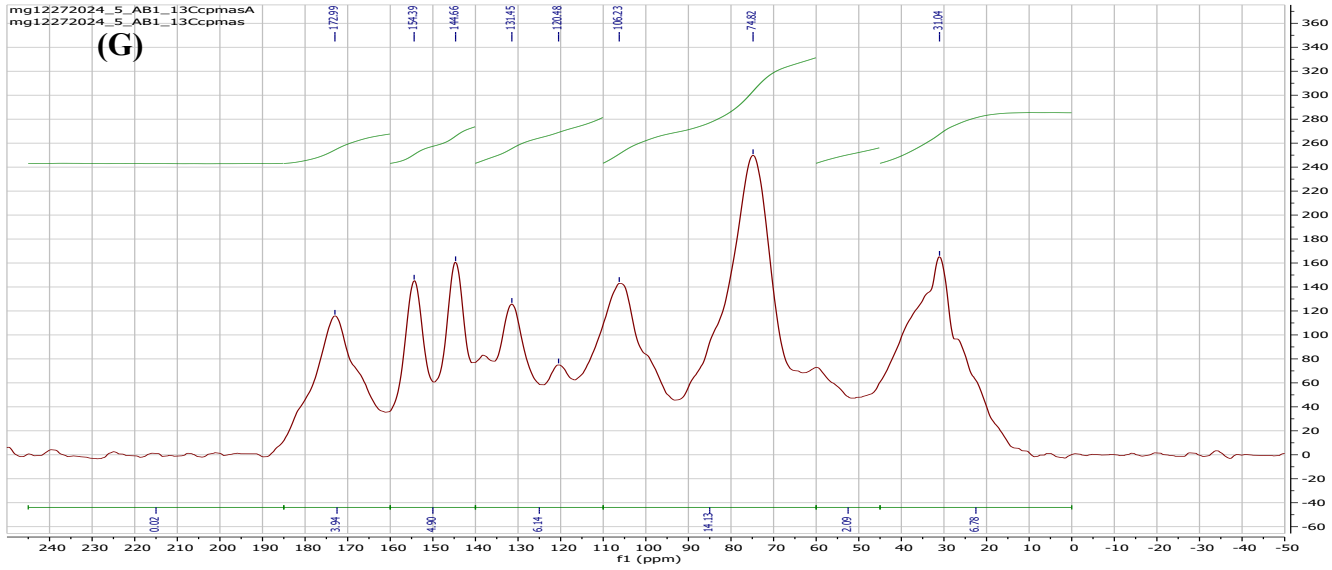

Figure S9. Continuation.

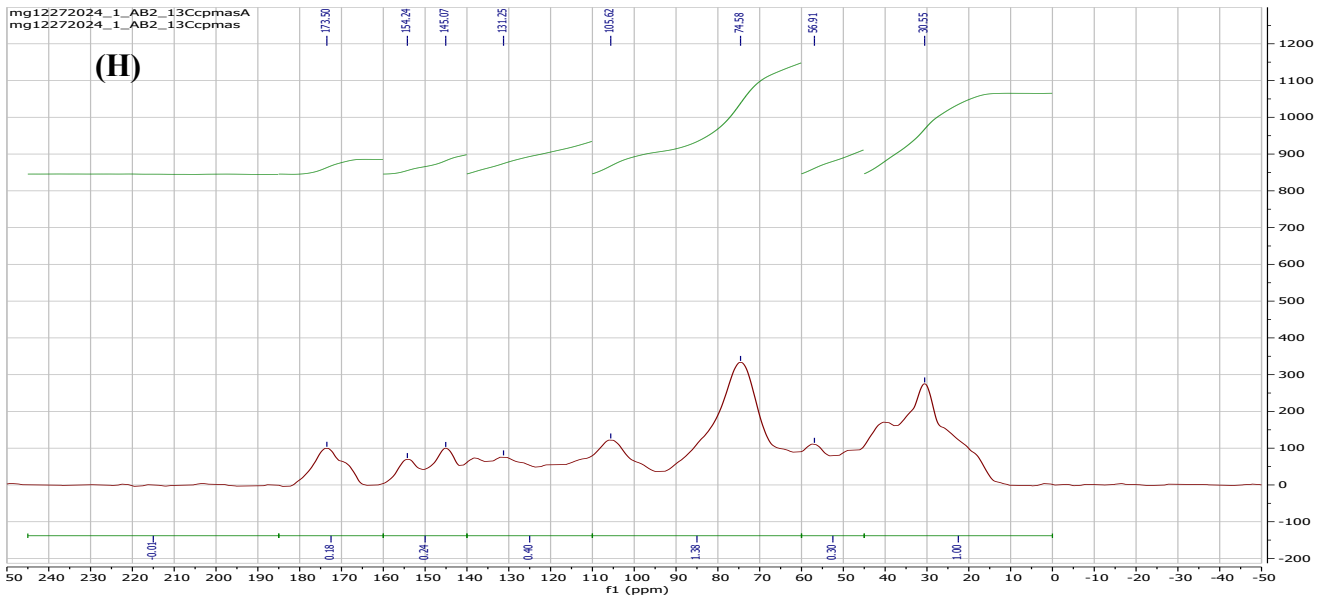

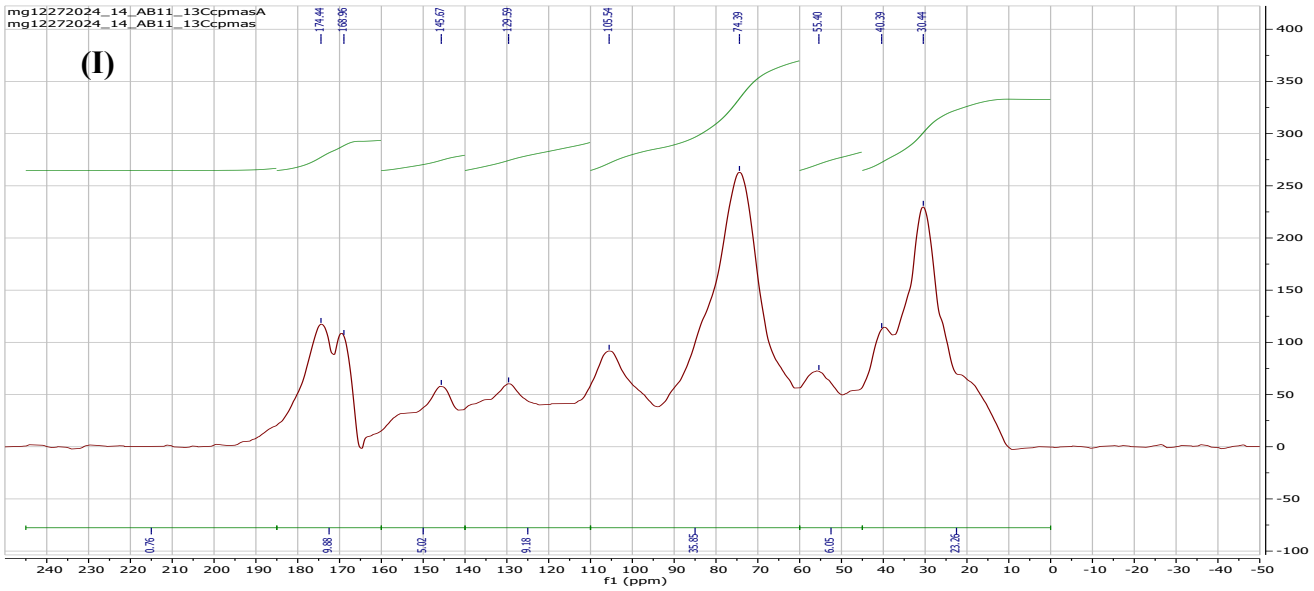

Figure S9. Continuation.

Furthermore, Table S8 presents the percentages of carbon functional groups detected in the six most efficient adsorbents and the three least sorptive ones.

Table S8. Distribution of carbon functional groups in the selected bioadsorbents based on ^{13}C CP/MAS NMR spectroscopy.

Adsorption-based selection	Samples	Alkyl-C%	O-Alkyl-C%	Aromatic-C	Carboxyl-C
Most adsorptive	**AF**	17	57	17	9
	AB	13	57	24	6
	EB	9	66	18	6
	OP	13	64	15	7
	AS	12	62	21	5
	DPS	6	60	26	7

	ZOB	26	47	16	11
Least adsorptive	**PGP**	20	41	29	10
	CGs	28	40	24	8

-According to the solid-state ^{13}C NMR spectra (Fig. S9) and the data in Table S8, it is shown that all investigated bioadsorbents exhibit the typical carbon distribution of agro-waste-derived materials, with resonances assigned to carbonyl carbons of carboxylic groups (170–180 ppm), aromatic carbons mainly from lignin (120–150 ppm), O-alkyl carbons of polysaccharides such as cellulose and hemicellulose (60–105 ppm), and aliphatic carbons associated with alkyl chains and lignin side groups (0–50 ppm). However, clear differences emerge when comparing the most adsorptive samples (EB, AF, AB, OP, AS, and DPS) with the least adsorptive ones (ZOB, PGP, and CGs). The former group is characterized by broader and more intense signals in O-alkyl (57-66 %) regions, indicating a higher abundance and/or greater accessibility of oxygen-containing functional groups, which are likely involved in covalent interactions with the antibiotic molecules. In particular, the pronounced carbohydrate (60–105 ppm) and carbonyl domains suggest favorable conditions for hydrogen bonding and electrostatic interactions, while the presence of aromatic carbons may further contribute through π-related interactions. In contrast, the least adsorptive samples (ZOB, PGP, and CGs) display sharper and less fluctuated signals in the key domains of carbons of O-Alkyl groups (40-47%), with comparatively lower relative intensities, pointing to a reduced availability or accessibility of reactive surface sites. This weaker involvement of oxygenated functional groups, together with a less favorable surface chemistry of these samples, is consistent with their lower adsorption capacities. Specifically, the lower porosity (17.6%) and *BET* surface area of CGs compared to ZOB, PGP explains its lower mean adsorption (30.31%) relative to the latter two (49.58% and 41.70%, respectively).
Overall, the NMR data highlight that variations in the relative contribution and accessibility of Carboxyl-C and O-Alkyl-C domains play a central role in governing the adsorption efficiency across the different bioadsorbents.

12. Desorption, hysteresis analysis, and adsorbent reusability

Fig. S10 shows the desorption curves, with data expressed in μmol kg^{-1}.

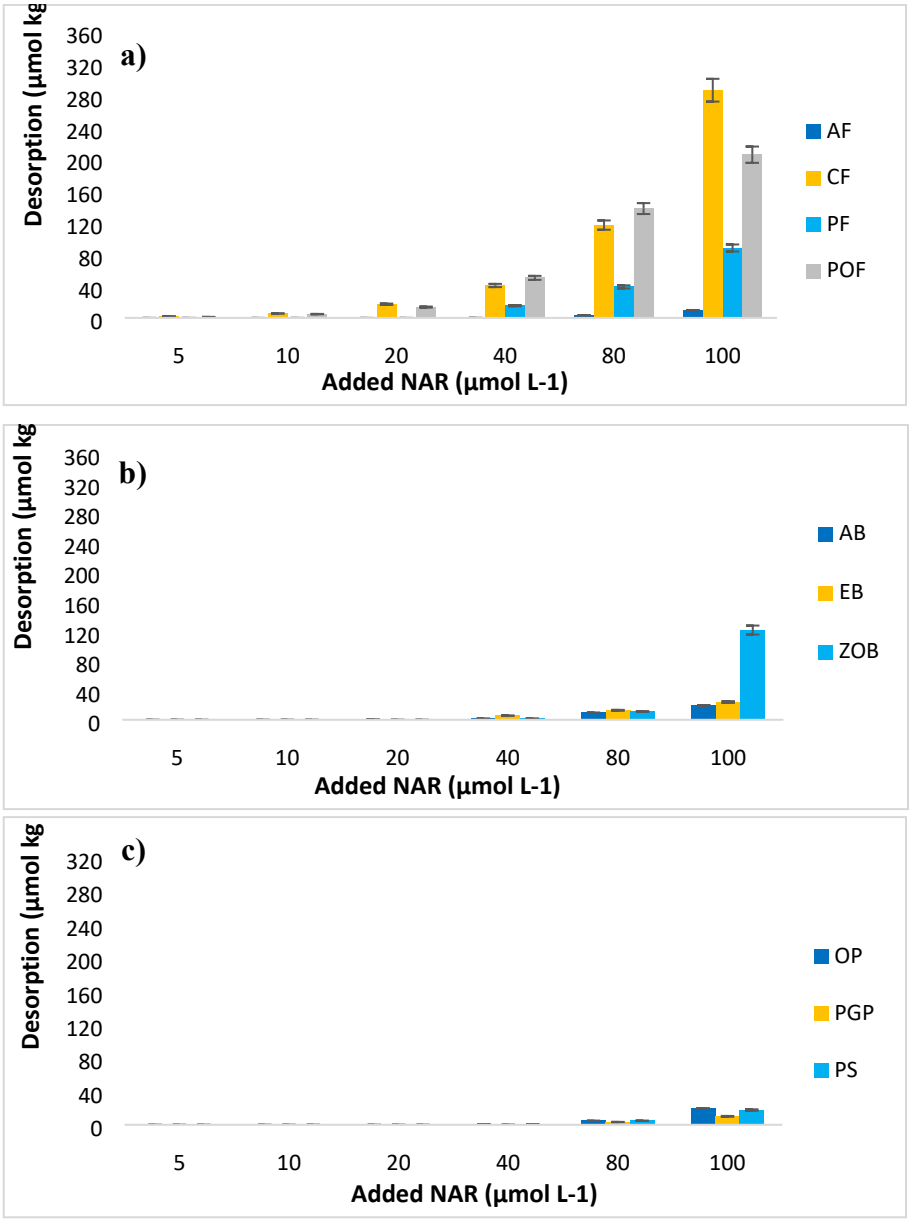

Figure S10. Desorption curves of narasin (NAR) (expressed in μmol kg^{-1}) for the natural fibers (a), barks (b), and the agro-food by-products (c,d), as a function of the antibiotic concentration added (μmol L^{-1}). Average values (n = 3), with coefficients of variation always <5%, and error bars represent the standard deviation.

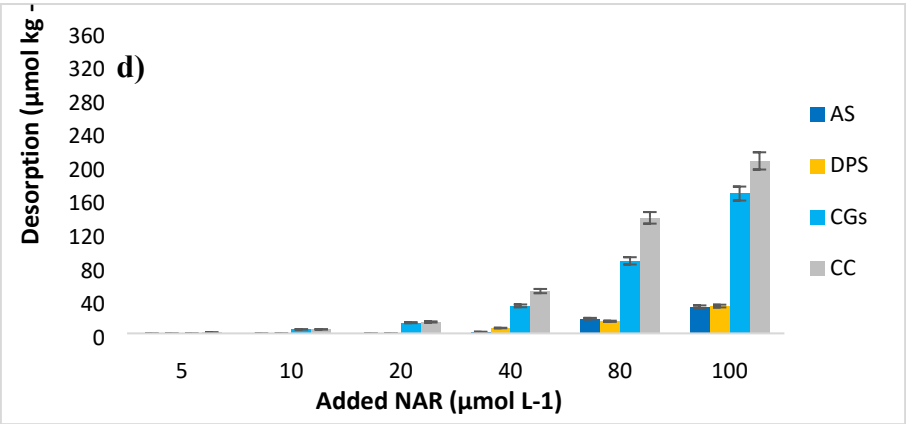

Figure S10. Continuation.

Table S9 lists the hysteresis index (*HI*) values for NAR desorption from the studied bioadsorbents at each of the initial antibiotic concentrations.

Table S9. Hysteresis index (*HI*) corresponding to the desorption of NAR from the bioadsorbents under investigation, and for each of the initial concentrations of the antibiotic added.

	By-products													
C_0 (µmol L^{-1})	**AF**	**CF**	**PF**	**POF**	**AB**	**EB**	**ZOB**	**OP**	**PGP**	**PS**	**AS**	**DPS**	**CGs**	**CC**
5	1	0.976	1	1	1	1	0	1	1	0	0	1	0	0.986
10	1	0.962	1	0.980	1	1	1	1	1	1	1	1	0.775	0.970
20	1	0.938	1	0.992	1	0.998	1	1	1	1	1	1	0.902	0.959
40	0.999	0.924	0.973	0.975	0.991	0.997	0.997	0.998	0.999	0.998	0.997	0.989	0.896	0.910
80	0.997	0.885	0.962	0.970	0.991	0.993	0.990	0.996	0.995	0.996	0.987	0.990	0.882	0.871
100	0.994	0.580	0.928	0.943	0.987	0.990	0.916	0.989	0.990	0.989	0.982	0.982	0.839	0.838
Average	0.998	0.877	0.976	0.976	0.995	0.996	0.817	0.997	0.997	0.830	0.828	0.993	0.715	0.992

Additionally, Fig. S11 represents the regeneration performance of the six most adsorptive by-products, showing NAR adsorption over six successive cycles using 0.01 M HCl for repeated desorption cycles followed by neutralization with NaOH. Experiments were conducted at unmodified (natural) pH and room temperature (25 ± 2 °C).

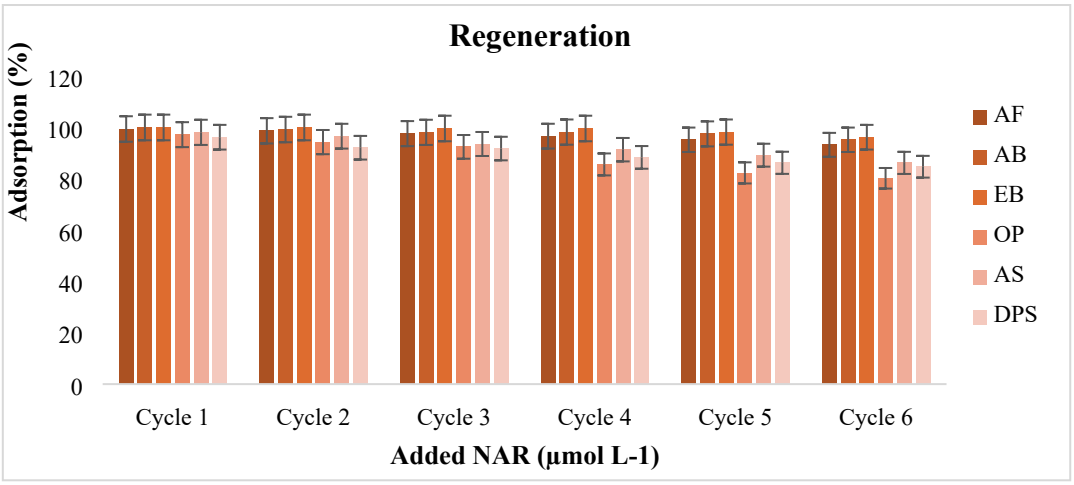

Figure S11. Adsorption of NAR onto the six most adsorptive by-products after six successive regeneration cycles using 0.01 M HCl, followed by neutralization with NaOH. Experiments were carried out at natural (unmodified) pH and at ambient temperature (25 ± 2 °C). Average values (n = 3), with coefficients of variation always <5%, and error bars represent the standard deviation.

References

1- Hussain SA, Prasher SO, Patel RM. Removal of ionophoric antibiotics in free water surface constructed wetlands. Ecol. Eng. 2012, 41:13-21. https://doi.org/10.1016/j.ecoleng.2011.12.006.

2- EFSA (European Food Safety Authority). Opinion of the scientific panel on contaminants in the food chain on a request from the European Commission on cross-contamination of non-target feeding stuffs by narasin authorised for use as a feed additive. EFSA J. 2007, 552:1-35.

3- Biswas S. Quantification of ionophore antimicrobials associated with poultry litter and their dynamics in soils of the mid-atlantic. Doctoral Thesis. University of Maryland, College Park ProQuest Dissertations and Theses 2014, 3682425.

4- Bak SA, Hansen M, Krogh KA, Brandt A, Halling-Sørensen B, Björklund E. Development and validation of an SPE methodology combined with LC-MS/MS for the determination of four ionophores in aqueous environmental matrices. Int. J. Environ. Anal. Chem. 2013, 93 :1500-1512. https://doi.org/10.1080/03067319.2013.763250.

5- Dusi G, Gamba V. Liquid chromatography with ultraviolet detection of lasalocid, monensin, salinomycin and narasin in poultry feeds using pre-column derivatization. J. Chromatogr. A. 1999, 835:243-246. https://doi.org/10.1016/S0021-9673(99)00044-8.

6- Rodríguez-López L, Santás-Miguel V, Cela-Dablanca R, Núñez-Delgado A, Álvarez-Rodríguez E, Pérez-Rodríguez P, Arias-Estévez M. Ciprofloxacin and trimethoprim adsorption/desorption in agricultural soils. Int. J. Environ. Res. Public Health. 2022, 19: 8426. https://doi.org/10.3390/ijerph19148426.

7- Sukul P, Lamshöft M, Zühlke S, Spiteller M. Sorption and desorption of sulfadiazine in soil and soil-manure systems. Chemosphere 2008, 73:1344-1350. https://doi.org/10.1016/j.chemosphere.2008.06.066.

8- Liang X, Liu L, Jiang Y, Nan Z, Deng X, Ma F, Wang G, Wu Y. Study of the sorption/desorption behavior of chlortetracycline on sediments in the upper reaches of the Yellow River. Chem. Eng. J. 2022, 428:131958-131968. https://doi.org/10.1016/j.cej.2021.131958.
9- Hamdi S, Issaoui M, Hammami S, Míguez-González A, Cela-Dablanca R, Barreiro A, Núñez-Delgado A, Álvarez-Rodríguez E, Fernández-Sanjurjo MJ. Removal of the highly toxic anticoccidial monensin using six different low-cost bio-adsorbents. Toxics 2024, 12:606-614. https://doi.org/10.3390/toxics12080606.
10-Hamdi S, Issaoui M, Hammami S, Míguez-González A, Cela-Dablanca R, Barreiro A, Núñez-Delgado A, Álvarez-Rodríguez E, Fernández-Sanjurjo M.J. Repurposing agro-food wastes to remove monensin from the environment. Euro-M editerr. J. Environ. Integr 2025a ,11:3.https://doi.org/10.1007/s41207-025-00979-9.
11-Hamdi S, Issaoui M, Hammami S, Míguez-González A, Cela-Dablanca R, Barreiro A, Núñez-Delgado A, Álvarez-Rodríguez E, Fernández-Sanjurjo M.J. Agro-waste materials: a low-cost approach to emerging contaminant mitigation. Bioresour. Technol. Rep 2025b, 32: 10241. https://doi.org/10.1016/j.biteb.2025.102412.
12- Blakemore LC. Exchange complex dominated by amorphous material (ECDAM). En: Smith, G.D. (Ed), The andisol proposal Edicion 1978, Soil Bureau, DSIR. New Zeland.
13- Bascomb C. Distribution of pyrophosphate-extractable iron and organic carbon in soils of various groups. Eur. J. Soil Sci. 1968, 19:251-268.
14- Van Soest PJ, Wine RH. Use of detergents in the analysis of fibrous feeds. IV. Determination of plant cell-wall constituents. J. Assoc. Off. Anal. Chem 1967, 50:50-55. https://doi.org/10.1093/jaoac/50.1.1.
15- Sluiter A, Hames B, Ruiz R, Scarlata C, Sluiter J, Templeton D, Crocker D. Determination of structural carbohydrates and lignin in biomass. National Renewable Energy Laboratory (NREL) Laboratory Analytical Procedure, 2012.
16- Boehm HP. Some aspects of the surface chemistry of carbon blacks and other carbons. Carbon 1994, 32:759-769. https://doi.org/10.1016/0008-6223(94)90031-0.
17- Goertzen SL, Thériault KD, Oickle AM, Tarasuk AC, Andreas HA. Standardization of the Boehm titration. Part I. CO_2 expulsion and endpoint determination. Carbon 2010, 48:1252-1261. https://doi.org/10.1016/j.carbon.2009.11.050.
18- Schonherr J, Buchheim JR, Scholz P, Adelhelm P. Boehm titration revisited (part I): Practical aspects for achieving a high precision in quantifying oxygen-containing surface groups on carbon materials. J. Carbon Res. 2018, 4:21-35. https://doi.org/10.3390/c4020021.
19- Kalijadis AM, Vukcevic MM, Jovanovic ZM, Lausevic ZV, Lausevic MD. Characterization of surface oxygen groups on different carbon materials by the Boehm method and temperature-programmed desorption. J. Serb. Chem. Soc. 2011, 76:757-768. https://doi.org/10.2298/JSC091224056K.
20-Chemical Book. Narasin 55134-13-9-Chemical Book. Retrieved March 10, 2025, from https://www.chemicalbook.com/ChemicalProductProperty_EN_CB3756283.htm.
21- EFSA (European Food Safety Authority). Safety and efficacy of Monteban® G100 (narasin) for chickens for fattening. EFSA J. 2018, 16: 1-38.2903/j.efsa.2018.5460.
22- Cataldo S, Gianguzza A, Milea D, Muratore N, Pettignano A, Sammartano S. A critical approach to the toxic metal ion removal by hazelnut and almond shells. Environ. Sci. Pollut. Res. 2018, 25:4238-4253. https://doi.org/10.1007/s11356-017-0779-3.
23- Reis N, Franca AS, Oliveira LS. Performance of diffuse reflectance infrared Fourier transform spectroscopy and chemometrics for detection of multiple adulterants in roasted and ground coffee. LWT-Food Sci. Technol. 2013 53:395-401. https://doi.org/10.1016/j.lwt.2013.04.008.

24- Zarrinbakhsh N, Wang T, Rodriguez-Uribe A, Misra M, Mohanty AK. Characterization of wastes and coproducts from the coffee industry for composite material production. Bioresources 2016, 11:7637-7653. https://doi.org/10.15376/biores.11.3.7637-7653.
25- Atabani AE, Mercimek SM, Arvindnarayan S, Shobana S, Kumar G, Cadir M, Al-Muhatseb AH. Valorization of spent coffee groundsrecycling as a potential alternative fuel resource in Turkey: an experimental study. J. Air Waste Manag. Assoc. 2018, 68:196-214. https://doi.org/10.1080/10962247.2017.1367738.
26- Ramos-Andrés M, Andrés-Iglesias C, García-Serna J. Production of molecular weight fractionated hemicelluloses hydrolyzates from spent coffee grounds combining hydrothermal extraction and a multistep ultrafiltration/diafiltration. Bioresour. Technol. 2019, 292: 121940-121952. https://doi.org/10.1016/j.biortech.2019.121940.
27- Martinek T, Riddell FG, Wilson CF. The conformations of narasin–metal complexes in solution determined by NMR spectroscopy. J. Chem. Soc. 2000, 2: 2192-2198. https://doi.org/10.1039/b005618i.